

# A Topological Approach to Gait Generation for Biped Robots

Nelson Rosa Jr. and Kevin M. Lynch

**Abstract**—This paper describes a topological approach to generating families of open- and closed-loop walking gaits for underactuated 2D and 3D biped walkers subject to configuration inequality constraints, physical holonomic constraints (e.g., closed chains), and virtual holonomic constraints (user-defined constraints enforced through feedback control). Our method constructs implicitly-defined manifolds of feasible periodic gaits within a state-time-control space that parameterizes the biped’s hybrid trajectories. Since equilibrium configurations of the biped often belong to such manifolds, we use equilibria as “templates” from which to grow the gait families. Equilibria are reliable seeds for the construction of gait families, eliminating the need for random, intuited, or bio-inspired initial guesses at feasible trajectories in an optimization framework. We demonstrate the approach on several 2D and 3D biped walkers.

## I. INTRODUCTION

A challenging problem in bipedal locomotion is the gait-generation problem: given a model of a bipedal robot, generate periodic gaits subject to the biped’s hybrid dynamics and other constraints. We present an approach to the gait-generation problem where equilibria of the biped are used as templates to find families of gaits. Under certain conditions, these equilibria can be continuously deformed into sets of walking gaits, including passive dynamic walking gaits (unactuated gaits where a biped walks downhill under the influence of gravity) and actuated gaits where the biped walks on flat ground or uphill.

In this paper, we assume the biped is physically symmetric about its sagittal plane, and we are interested in symmetric *period-one* gaits: periodic gaits where each step by the right leg is identical and the mirror image of steps by the left leg.<sup>1</sup> Given the hybrid dynamics of the biped, the entire trajectory of a single step is represented by the finite-dimensional tuple  $c = (x_0, \tau, \mu) \in \mathcal{S} = \mathcal{X} \times \mathbb{R} \times \mathcal{M} \subset \mathbb{R}^{2n+1+k}$ , where  $x_0 = (q_0, \dot{q}_0) \in \mathcal{X} \subseteq \mathbb{R}^{2n}$  is the initial state of the biped with configuration  $q_0 \in \mathcal{Q} \subseteq \mathbb{R}^n$ ;  $\tau \geq 0$  is the duration of the step; and  $\mu \in \mathcal{M} \subseteq \mathbb{R}^k$  describes design or control parameters, such as  $k$  polynomial coefficients describing feedback-control-enforced coupling between joints of the biped. Our goal is to find points in  $\mathcal{S}$  that correspond to period-one gaits.

N. Rosa and K. M. Lynch are with the Department of Mechanical Engineering and the Center for Robotics and Biosystems; K. M. Lynch is also with the Northwestern Institute on Complex Systems, Northwestern University, Evanston, IL 60208. {nr} at u.northwestern.edu, {kmlynch} at northwestern.edu

This work was supported by NSF grants IIS-0964665, IIS-1018167, and CMMI-1436297.

<sup>1</sup>The approach can be extended to general period- $n$  gaits, such as limping gaits [1], but in this paper we focus on period-one gaits for simplicity.

To precisely define period-one gaits, we define the flow  $\varphi$  such that  $\varphi_\mu^\tau(x_0)$  is the biped’s state after time  $\tau$  using the controls  $\mu$  beginning from the state  $x_0$ . We define the coordinate-flip operator  $\text{flip} : \mathcal{X} \rightarrow \mathcal{X}$  that maps a state of the biped to its symmetric state (i.e., the equivalent state when the other leg is taking a step). The flip operator satisfies  $\text{flip}(\text{flip}(x_0)) = x_0$ . With these definitions, a point  $c = (x_0, \tau, \mu) \in \mathcal{S}$  corresponds to a period-one gait if and only if  $\varphi_\mu^\tau(x_0) - \text{flip}(x_0) = 0$ .

Said another way, the *periodicity map*  $P : \mathcal{S} \rightarrow \mathcal{X}$  is defined as

$$P(c) = \varphi_\mu^\tau(x_0) - \text{flip}(x_0),$$

and the set of all period-one gaits, denoted  $\mathcal{G}$ , is the set of all points  $c \in \mathcal{S}$  satisfying  $P(c) = 0$ , i.e.,  $\mathcal{G} = P^{-1}(0)$ . Since  $P(c) = 0$  specifies  $2n$  constraints on the  $(2n+k+1)$ -dimensional space  $\mathcal{S}$ , in general we would expect  $\mathcal{G}$  to be  $(k+1)$ -dimensional ( $\dim(\mathcal{S}) - \dim(P)$ ).

The goal of our work is not to find a single period-one gait (a single point in  $\mathcal{G}$ ), but to map out a “large” continuous family of gaits  $\mathcal{G}_{\text{mapped}} \subset \mathcal{G} \subset \mathcal{S}$ . The set of gaits  $\mathcal{G}_{\text{mapped}}$  may include walking downhill, walking uphill, and even hand-to-hand gibbon-like swinging gaits (*brachiation*) underneath a support. A long-term goal is a full topological description of  $\mathcal{G}$  for a given state-time-control space  $\mathcal{S}$ , but that is beyond the scope of this paper.

The standard approach to finding a single gait in  $\mathcal{G}$  is to formulate a non-convex optimization problem (OP) in the parameters  $x_0$ ,  $\tau$ , and  $\mu$ . The convergence of non-convex OPs relies critically on the initial seed value [2], [3], which is typically chosen randomly or by applying domain-specific knowledge [3]–[6]. No general guidelines exist for generic  $n$ -degree-of-freedom bipeds.

In our framework, however, any one-footed rest state  $x_{\text{eq}} = (q_{\text{eq}}, 0)$  which is also an equilibrium (i.e.,  $\varphi_\mu^t(x_{\text{eq}}) = x_{\text{eq}}$  for some  $\mu$  and all  $t \geq 0$ ) is trivially an “equilibrium gait”  $c_{\text{eq}} = (x_{\text{eq}}, \tau, \mu)$ . A subset of these equilibrium gaits are period-one gaits satisfying  $P(c_{\text{eq}}) = 0$ . The set of all such trivial, non-locomoting equilibrium period-one gaits is denoted  $E$ , a subset of  $\mathcal{G}$ . An equilibrium gait  $c_{\text{eq}}$  is often in the same connected component of  $\mathcal{G}$  as useful locomoting gaits, and this motivates the use of numerical continuation methods (NCMs) to generate this connected component starting from  $c_{\text{eq}}$ . In particular, branches of locomoting gaits intersect an equilibrium branch containing  $c_{\text{eq}}$  on the connected component at critical values of the step duration and fixed values of  $(x_{\text{eq}}, \mu)$  where the rank of the Jacobian of  $P$  at these values is not maximal. In other words, the easy-to-find equilibria

are seeds, or “templates,” which are continuously deformed to generate  $\mathcal{G}_{\text{mapped}}$ .

Having a continuous family of gaits  $\mathcal{G}_{\text{mapped}}$ , instead of one or a small number of gaits, can be useful in a number of ways. First, some high-level walking motion planners rely on low-level gait-generation modules, or a pre-computed library of gaits, that can be applied on different terrains [7]–[10]. A gait family  $\mathcal{G}_{\text{mapped}}$  constructed using our approach is a continuous version of a gait library. Second, a gait family  $\mathcal{G}_{\text{mapped}}$  allows the possibility of design of control laws that drive the biped to  $\mathcal{G}_{\text{mapped}}$  rather than to a single specific gait  $c \in \mathcal{G}$ . In general, it is easier to design a controller to stabilize a manifold than to stabilize a point. Most importantly,  $\mathcal{G}_{\text{mapped}}$  provides a global view of the possible gaits of a biped robot for the given space of design and control parameters  $\mathcal{M}$ .

#### A. Statement of Contributions

This paper describes a topological approach to generating families of walking gaits for 2D and 3D underactuated biped walkers with point, curved, or flat feet that are physically symmetric about their sagittal plane. We use NCMs to map out connected components of gaits in a state-time-control space  $\mathcal{S}$ . The biped may be subject to configuration inequality constraints, physical holonomic constraints (PHCs) such as closed chains, and virtual holonomic constraints (VHCs), i.e., user-defined constraints enforced through feedback control. Our main contributions are:

- 1) **A topological approach to the gait-generation problem.** We view gaits as points in a space  $\mathcal{S}$  of parameterized trajectories, where we explore a fundamental property of the periodic orbits of a biped’s hybrid dynamics: their connectivity to each other in  $\mathcal{S}$  across variations in state, step duration, and design and control parameters.
- 2) **The use of equilibria to generate a continuum of walking gaits.** We prove that we can find families of locomoting gaits that transversally intersect a family of equilibrium gaits in  $\mathcal{E}$  at points  $c_{\text{eq}} = (x_{\text{eq}}, \tau, \mu)$  for a given fixed pair  $(x_{\text{eq}}, \mu)$ . We provide an algorithm for determining the values of  $\tau$  where the intersections occur.
- 3) **A framework for generating open-loop periodic motions that satisfy the full hybrid dynamics.** We address the open problem [2] of generating open-loop periodic motions for the unactuated joints of a biped robot subject to PHCs and VHCs, including when all joints are unactuated (passive dynamic walking) and when a subset of joints track parameterized trajectories.

This paper builds on our conference paper [11] and the abstract [12]. In this previous work, we introduced the concept of using numerical continuation methods (NCMs) to generate gaits for bipeds, including those subject to virtual holonomic constraints. This paper extends our preliminary work in several important ways: 1) we provide a unified framework for generating gaits from equilibrium templates for 2D and 3D underactuated bipeds subject to configuration inequality constraints and physical and virtual holonomic constraints; 2) we provide a new algorithm to find specific types of gaits with desired properties; and 3) we provide applications of the

framework to finding gaits for simulated complex 3D bipeds such as Atlas and MARLO.

#### B. Related Work

The use of equilibria for generating families of unactuated walking gaits can be found in past works studying simple two- and three-degree-of-freedom passive dynamic walking biped models [13]–[15]. The solution families of walking gaits for these biped models converge to an equilibrium gait because the solution families exhibit a vanishing step size—as the biped’s walking slope approaches flat ground, the step size of the corresponding gait becomes shorter. In the limit, as the incline approaches level ground, the state of the biped must approach an equilibrium gait [16], a “gait” with zero step size. The work in [17] explores this notion of finding periodic walking motions near equilibria for simple walking models with vanishing step sizes. The paper gives necessary conditions on the physical parameters of planar two- and three-link bipeds for walking at arbitrarily small but near-zero slopes.

We extend the work on unactuated, low-dimensional, planar bipeds with vanishing step sizes to include powered high-degree-of-freedom 2D and 3D bipeds. In our previous work [11], [18], [19], we used NCMs [20] to generate families of open-loop walking and brachiating gaits that utilize the “natural” or full dynamics of the biped model. In particular, [11] demonstrates that equilibria of representative point-feet planar bipeds can be continuously deformed into families of passive dynamic walking gaits. We extend this body of work to include closed-loop gaits for underactuated bipeds using the hybrid zero dynamics (HZD) framework [21]–[23].

The HZD framework is an experimentally-validated approach to generating stable walking gaits for underactuated bipedal robots subject to virtual constraints (constraints on the biped that are imposed using feedback control) [5], [24], [25]. The notion of virtual constraints, in particular virtual *holonomic* constraints (VHCs), has been a useful concept in the design and control of bipedal walking gaits. We enforce VHCs using an HZD controller, which can provably impose the constraints under mild conditions [21]. Alternative control schemes for enforcing a set of VHCs also exist [26].

A common application of VHCs on a bipedal system is to couple the motion of a subset of joints on an underactuated robot so that they evolve with respect to a function of the biped’s configuration as opposed to time. The resulting motion is then synchronized to, for example, the motion of a biped’s center of mass projected onto its transverse plane when the constraints are properly enforced through feedback control. The net effect is that the biped’s joints move only if the center of mass moves, irrespective of time. In such a case, the motions are said to be self-clocking [24].

Given a biped subject to physical and virtual holonomic constraints, we generate gaits using NCMs, which originate from results in topology and differential geometry [27]. In this context, our application is similar to tracing the points on a differentiable manifold (e.g., a curve or a higher-dimensional surface) represented as a set of equations that are continuously differentiable. Applications of continuation methods for generating dynamic motions can be found in [28], [29].

NCMs are also present in optimization solvers, which many gait-generation libraries rely on to generate gaits. NCMs are typically used to find feasible solutions (e.g., elastic mode in SNOPT [30]) or to solve a series of related optimization problems (e.g., interior-point methods [31], like IPOPT).

The standard approach to solving the gait generation problem is to formulate it as an optimization problem (OP) [6], [32], [33]. The idea is to specify the decision variables, constraints, and objective function used in the optimization in such a way that the underlying solver (often SNOPT, IPOPT, or fmincon) can quickly and robustly converge from an arbitrary seed value [3], [5], [6]. Recent approaches use direct collocation methods as part of the problem formulation, where the biped's equations of motion are discretized into a set of algebraic constraints using a low-order implicit Runge-Kutta scheme with fixed step size. A comparable optimization-based framework to our work is [32]. In [32], direct collocation methods are used to generate gaits for bipeds subject to VHCs using an HZD feedback controller to enforce the VHCs.

Our use of NCMs to find gaits differs from methods in the literature that rely on OPs in that these works attempt to find the “best” gait while we use NCMs to find many gaits without having to guess an initial seed value.

### C. Paper Outline

After covering mathematical preliminaries in Section II, we describe the gait space  $\mathcal{G}$  and how to generate gaits from equilibria using NCMs in Sections III–IV. In Section V, we give examples of generating gaits for the planar compass-gait walker and the 3D bipeds Atlas and MARLO.

We also provide supplementary downloadable material [34]. The material consists of

- 1) an MP4 video of walking animations of all biped models used in this paper,
- 2) a Mathematica v11.0.3 library of our framework and implementation details of the models, and
- 3) a Node.js v12.17.0 visualization library for animating and creating video clips of the gaits.

## II. PRELIMINARIES

In this section, we specify the biped's hybrid dynamics, give the problem statement, state assumptions, and formally define the space of parameterized trajectories  $\mathcal{S}$ , the gait space  $\mathcal{G}$ , and the connected components of  $\mathcal{G}$ .

### A. The Hybrid Dynamics

The *hybrid dynamics*  $\Sigma$  of an  $n$ -degree-of-freedom biped robot is the tuple  $\Sigma = (\mathcal{X}, f, \Delta, \phi)$ , where

- $\mathcal{X}$  is the biped's state space;
- $f(x, u) \in T\mathcal{X}$  describes the continuous dynamics, where  $u \in \mathbb{R}^{n_u}$  is the robot controls;
- $\Delta : \mathcal{X} \rightarrow \mathcal{X}$  is a jump map to model instantaneous impacts; and
- $\phi : \mathbb{R} \times \mathcal{X} \rightarrow \mathbb{R}$  is a switching function to indicate when a foot hits the ground. If  $\phi(t, x) = 0$ , then  $t \in \mathbb{R}$  is a

*switching time*,  $x \in \mathcal{X}$  is a *pre-impact state*, and the foot is in contact with the ground.

The motion of the biped can be subject to  $n_p$  physical holonomic constraints (PHCs) and  $n_v$  virtual holonomic constraints (VHCs). The physical constraints, due to closed-loop linkages or kinematic constraints between the foot and the ground, for example, give rise to  $n_p$  constraint forces. The virtual constraints are enforced using feedback control. We assume that the biped has  $n_u$  ( $n_u \geq n_v$ ) control inputs  $u(t) \in \mathbb{R}^{n_u}$  to enforce the VHCs in the system.

The VHCs specify the configuration of certain degrees of freedom of the biped as a function of a *phase variable*  $\theta$ . In real-time control, the phase variable is often a function of the biped's state [21] (e.g., the swing leg's joints could be “clocked” by the angle from the stance foot to the hip), but to plan a single step of a gait, time suffices as a phase variable.

In this paper, a VHC takes the generic form

$$q_i(t) - b_i^d(\theta(t), a) = 0, \quad t \in [0, \tau], \quad (1)$$

where  $\tau$  is the step duration,  $\theta(t) = t/\tau \in [0, 1]$  is the phase variable,  $q_i(t) \in \mathbb{R}$  is a joint angle ( $1 \leq i \leq n$ ),  $b_i^d(\theta(t), a) \in \mathbb{R}$  is a Bézier polynomial of degree  $d \in \mathbb{N}$ , and  $a \in \mathbb{R}^{n_a}$  is a vector of polynomial coefficients. Appendix A provides further modeling details, including how to enforce a set of VHCs.

### B. The Space of Parameterized Trajectories

Given  $\Sigma$ , we are interested in hybrid trajectories that correspond to a step of a biped of the form

$$x(\tau) = \varphi_\mu^\tau(x_0) = \Delta(x_0; \mu) + \int_0^\tau f(\varphi_\mu^t(x_0), u; \mu) dt, \quad (2)$$

where  $x_0 \in \mathcal{X}$  is the pre-impact state at  $t = 0$ ,  $\varphi_\mu^t(x_0) \in \mathcal{X}$  is the state of the robot at time  $t$ ,  $\varphi_\mu^\tau(x_0)$  is the next pre-impact state at  $t = \tau \geq 0 \in \mathbb{R}$ ,  $\mu \in \mathcal{M}$  is a vector of input parameters, and  $u(t) \in \mathbb{R}^{n_u}$  is a vector of control inputs that depend on  $\mu$ . The parameters  $x_0$ ,  $\tau$ , and  $\mu$  define the space of parameterized trajectories.

*Remark 1.* The input parameters  $\mu$  can be used to specify design parameters of the biped such as the center of mass position of a link, leg length, spring coefficients, and moment of inertia. It can also be used to define control parameters, like feedback gains, magnitude of ankle push-off force, and spline coefficients.

**Definition 1.** A biped's *state-time-control space*  $\mathcal{S}$  is a finite-dimensional vector space  $\mathcal{S} \subseteq \mathcal{X} \times \mathbb{R} \times \mathcal{M} \subset \mathbb{R}^{2n+1+k}$ . A point  $c \in \mathcal{S}$ , where  $c = (x_0, \tau, \mu)$ , defines a hybrid trajectory  $x(t) \in \mathcal{X} \subseteq \mathbb{R}^n$  given input parameters  $\mu \in \mathcal{M} \subseteq \mathbb{R}^k$  starting from  $x_0 \in \mathcal{X}$  at switching time  $t = 0$  until the next switching time  $\tau > 0$ .

Figure 1 shows how the parameters of the state-time-control space  $\mathcal{S}$  can affect the motion of an  $n$ -degree-of-freedom biped robot. As defined earlier, the set of all period-one gaits in  $\mathcal{S}$  is defined using the periodicity map  $P$  as

$$\mathcal{G} = \{c \in \mathcal{S} : P(c) = 0\},$$

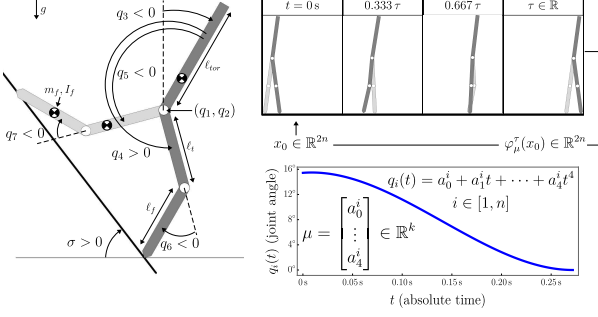


Fig. 1. A generic  $n$ -degree-of-freedom biped model (left). We parameterize motions that satisfy the model's hybrid dynamics (top right) with a pre-impact state  $x_0 \in \mathcal{X} \subseteq \mathbb{R}^{2n}$ , a switching time  $\tau \in \mathbb{R}$ , and a vector of input parameters  $\mu \in \mathcal{M} \subseteq \mathbb{R}^k$  (top and bottom right). We use the vector  $\mu$  to represent any parameter that is not a state or switching time. In this example, the vector  $\mu$  consists of  $k$  polynomial coefficients (bottom right) used to define the trajectory of joint  $q_i$  of the biped.

i.e., the set of all points  $c = (x_0, \tau, \mu)$  satisfying  $\varphi_\mu^\tau(x_0) - \text{flip}(x_0) = 0$ . The set of equilibrium (stationary) gaits is defined as

$$E = \{c_{\text{eq}} = (x_{\text{eq}}, \tau, \mu) \in \mathcal{G} : f(x_{\text{eq}}, u(t); \mu) = 0 \ \forall t \in \mathbb{R}\},$$

i.e., the set of all points  $c_{\text{eq}}$  satisfying  $P(c_{\text{eq}}) = 0$  and  $\varphi_\mu^t(x_{\text{eq}}) = x_{\text{eq}}$  for all  $t$ .

### C. The Connected Components of the Gait Space $\mathcal{G}$

**Definition 2.** Let  $\mathcal{G}$  be the space of all gaits in  $\mathcal{S}$ .

- 1) A path between two points  $a$  and  $b$  in  $\mathcal{G}$  is a continuous function  $p : [0, 1] \rightarrow \mathcal{G}$  such that  $p(0) = a$  and  $p(1) = b$ .
- 2) A set  $X \subseteq \mathcal{G}$  is path-connected if for all  $a, b \in X$ , there exists a path  $p : [0, 1] \rightarrow X$  with  $p(0) = a$  and  $p(1) = b$ .
- 3) A set  $X \subseteq \mathcal{G}$  is a connected component of  $\mathcal{G}$  if  $X$  is path-connected and  $X$  is maximal with respect to inclusion.

**Theorem 1.** [35] Let  $D$  be an open set in  $\mathcal{G}$  and the periodicity map  $P : \mathcal{S} \rightarrow \mathbb{R}^{2n}$  be a class  $\mathcal{C}^r$  differentiable function. If for every  $c \in D$ , the Jacobian  $J(c) \in \mathbb{R}^{2n \times (2n+k+1)}$

$$J(c) = \frac{\partial P}{\partial c}(c) = \left[ \frac{\partial \varphi}{\partial x}(c) - I_{2n}, \quad \frac{\partial \varphi}{\partial \tau}(c), \quad \frac{\partial \varphi}{\partial \mu}(c) \right] \quad (3)$$

has maximal rank  $2n$ , then  $D$  is a  $(k+1)$ -dimensional ( $\mathcal{C}^r$  differentiable) manifold in  $\mathcal{G}$ .

For a point  $c_0 \in \mathcal{G}$ , we have from [20], [36]

$$T_{c_0} \mathcal{G} = \text{Null}(J(c_0)), \quad (4)$$

where  $\text{Null}(J(c_0))$  is the null space of  $J$  from Equation (3) and  $T_{c_0} \mathcal{G}$  is the tangent space of  $\mathcal{G}$  at  $c_0$  [37].

**Definition 3.** A point  $c \in P^{-1}(0)$  is a singular point of  $P$  if  $\text{rank}(J(c)) < 2n$ . Points are regular if they are not singular.

The connected components of  $\mathcal{G}$  generally consist of submanifolds of  $\mathcal{S}$  glued together at singular points of the periodicity map  $P$ .

### D. Problem Statement

Given

- a hybrid model  $\Sigma = (\mathcal{X}, f, \Delta, \phi)$  of a biped,
- a finite-dimensional space  $\mathcal{S}$  of parameterized trajectories,
- an implicit description of the set of all gaits  $\mathcal{G} \subseteq \mathcal{S}$  as the points  $c$  in  $P^{-1}(0)$ , and
- a description of the set of equilibria  $E \subset \mathcal{G}$ ,

use NCMs to approximately trace the connected components of  $\mathcal{G}$  that contain  $E$ . The constructed set is denoted  $\mathcal{G}_{\text{mapped}}$ .

### E. Assumptions

**Assumption 1.** Unless otherwise stated, we assume

- A1 Bipeds are physically symmetric about their sagittal plane.
- A2 Bipeds undergo exactly one collision per step, a plastic impact between the pre-impact swing leg and the ground. At impact, the pre-impact stance leg breaks contact with the ground, and there is no free-flight phase (the stance leg instantaneously changes at impact). No slipping occurs at contacts between a foot and the ground.
- A3 The next foot hits the support surface after a specified period of time has elapsed, i.e., the impact is based on time, not state.
- A4 Bipeds may be subject to physical and virtual holonomic constraints, but not nonholonomic constraints.

Assumptions A1–A2 allow us to take advantage of a biped's symmetry to define a gait after one step with only one impact. Additional impacts would be needed to model the knees of a walker hitting a mechanical stop to prevent hyperextension [4], [38]. Assumption A2 also rules out heel-toe collisions for bipeds with non-point feet [32], [33]. This is a common assumption for point-, curved-, and flat-footed walkers (i.e., all contact points on the bottom of a foot impact the ground at the same time).

Given Assumption A3, the hybrid dynamics  $\Sigma = (\mathcal{X}, f, \Delta, \phi)$  with fixed switching times is

$$\Sigma : \begin{cases} \dot{x}(t) = f(x(t), u(t)) & t \neq k\tau, \\ x(t^+) = \Delta(x(t^-)) & t = k\tau, \end{cases} \quad (5)$$

where  $x(t) \in \mathcal{X}$ ,  $f(x, u) \in T\mathcal{X}$ , and  $\Delta(x) \in \mathcal{X}$  are the state of the robot at time  $t$ , a vector field, and a jump map, respectively (see Equation (2)),  $x(t^-)$  and  $x(t^+)$  are pre- and post-impact states, respectively, and  $k \geq 0 \in \mathbb{Z}$  is the  $k^{\text{th}}$  impact. The switching function  $\phi$  is  $\phi(t, x) = t - k\tau$ .

Finally, Assumption A4 precludes the use of virtual nonholonomic constraints as discussed in [22].

### III. THE BASIC GAIT-GENERATION APPROACH

We now present the core concepts and algorithms behind our framework. Specifically, we

- 1) describe the connected components of  $\mathcal{G}$  that include equilibrium gaits (EGs) (Section III-A),
- 2) describe how to find paths from an EG  $c_{\text{eq}} \in E \subseteq \mathcal{G}$  to a set of nonstationary gaits (nontrivial periodic orbits of the hybrid dynamics) in  $\mathcal{G} - E$  (Section III-B),

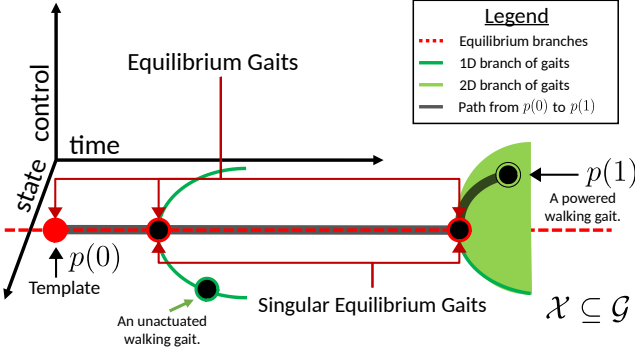


Fig. 2. A conceptual illustration of a portion of a connected component of gaits  $\mathcal{X}$  in  $\mathcal{G} \subset \mathcal{S}$  of a biped. The singular points, 1D curves, and surface emanating from the rightmost singular point depicts the full two-dimensional connected component. The rest of the figure depicts gaits in a 1D slice (constant state and control) of the connected component. This (user-defined) slice is used to search for singular equilibrium gaits and construct the initial set of gaits for  $\mathcal{G}_{\text{mapped}}$ .

- 3) present a continuation method for tracing curves (one-dimensional manifolds) in  $\mathcal{G}$  (Section III-C),
- 4) present an algorithm for constructing one-dimensional slices of  $\mathcal{G}$  from EGs (Section III-D), and
- 5) give an illustrative example of the basic approach using the compass-gait walker (Section III-E).

#### A. Connected Components of $\mathcal{G}$ Containing Equilibrium Gaits

The space of gaits  $\mathcal{G}$  in the state-time-control space  $\mathcal{S}$  may consist of multiple separate connected components. We are particularly interested in those connected components that include equilibrium gaits (EGs). A biped standing still on one foot is an example of an EG.

Figure 2 is a conceptual depiction of a connected component of an EG for an  $n$ -degree-of-freedom biped walker with one switching time and  $k = 1$  design and control parameters. The dimension of  $\mathcal{S}$  is  $2n + k + 1 = 2n + 2$  and the dimension of the manifolds in  $\mathcal{G}$  are  $\dim(\mathcal{S}) - 2n = k + 1 = 2$ -dimensional. Examples of manifolds in the figure are the red-dashed and green curves (1D slices of a larger 2D manifold) and the green surface (a 2D manifold). There are two singular points depicted as black dots with thick red borders.

The task is to find paths from an EG in  $E$  to a set of gaits in  $\mathcal{G} - E$  on the EG's connected component. An EG in the gait space  $\mathcal{G}$  is always a part of a continuum of EGs of the form  $(x_{\text{eq}}, \tau, \mu)$ , where  $x_{\text{eq}}$  and  $\mu$  are fixed and  $\tau$  can take any nonnegative value ( $\tau \geq 0$ ). A path-connected set of EGs that are regular points of the periodicity map  $P$  form an *equilibrium branch* (red dashed line in Figure 2) on the connected component. Equilibrium branches reside in constant-control slices of  $\mathcal{S}$ .

In a constant-control slice of  $\mathcal{S}$ , an equilibrium branch of a gait connected component often intersects with a branch of walking gaits also residing in the slice. The point of intersection can only happen at EGs that are singular points of  $P$ . For example, at singular EGs in Figure 2, we can switch onto a non-equilibrium branch of gaits and trace the branch consisting of walking gaits (dark green curves) for inclusion

in  $\mathcal{G}_{\text{mapped}}$ . These gaits can then be used to add gaits not in the constant-control slice (gaits on the green surface).

We specify a constant-control slice of  $\mathcal{G}$  with the map  $M_0 : \mathcal{S} \rightarrow \mathbb{R}^{2n+k}$

$$M_0(c) = [P^T(c), \Phi_0^T(c)]^T, \quad \Phi_0(c) = \mu - \mu_0, \quad (6)$$

where  $\mathcal{G}_0 = M_0^{-1}(0) \subset \mathcal{S}$  is the set of gaits of  $M_0$  and the  $k$  auxiliary constraints  $\Phi_0(c) = 0$  keep the controls constant at  $\mu_0$ . In other words,  $\mathcal{G}_0$  lives in a constant-control slice of  $\mathcal{S}$  (the red and dark green curves in Figure 2). The set of equilibrium gaits of  $M_0$  is  $E_0 = E \cap \mathcal{G}_0$ . We specify how to find singular EGs in  $E_0$  in the next section. In general, we use the subscript 0, as in  $M_0$ , for variables related to a constant-control slice  $\mathcal{G}_0$  in  $\mathcal{G}$ .

**Remark 2.** Equilibrium branches only exist because we assume a robot's swing foot can impact the ground at any time. Under any state-based switching strategy, equilibria are either isolated points in  $\mathcal{G}$ , or not in  $\mathcal{G}$  at all, depending on whether conditions placed on the switching function  $\phi$  allow for infinite impacts in zero time [39].

**Remark 3.** The locations of singular EGs on a connected component are determined by the kinematic and dynamic properties of the biped. Any changes to the biped model, for example, the addition of physical or virtual holonomic constraints, modifications to the control inputs  $u$ , or changing the biped's total mass, can shift the singular points or change the number of singular points on the connected component.

#### B. Detecting Singular Equilibrium Gaits

Given the characterization of equilibrium gaits (EGs) in Section III-A, consider the set of EGs  $\{c_{\text{eq}} = (x_{\text{eq}}, \tau, \mu) \mid \tau > 0\}$  for fixed control inputs  $\mu$ . For this set, the indicator function

$$I(\tau) = \det \left( \frac{\partial P}{\partial x_0}(x_{\text{eq}}, \tau, \mu) \right) \quad (7)$$

can be used to identify singular EGs by searching along the switching-time axis for values of  $\tau$  that make  $I(\tau)$  zero.

Given the map  $M_0$  (Equation (6)) and the Jacobian of  $M_0$ ,

$$J_0(c) = \begin{bmatrix} \frac{\partial P}{\partial c}(c) \\ \frac{\partial \Phi_0}{\partial c}(c) \end{bmatrix} = \begin{bmatrix} \frac{\partial P}{\partial x_0}(c) & \frac{\partial P}{\partial \tau}(c) & \frac{\partial P}{\partial \mu}(c) \\ 0 & 0 & I_k \end{bmatrix}, \quad (8)$$

the next two propositions prove that we can find a path from an equilibrium point  $c_{\text{eq}} \in E_0$  to a set of gaits in  $\mathcal{G}_0 - E_0$  by searching for singular EGs in  $E_0$ . In the first proposition, we establish the existence of 1D equilibrium branches in  $\mathcal{G}_0$ , which leads to a corollary that gives the condition for when an EG is a regular point of  $M_0$ .

#### Proposition 1. Given

- 1) a biped's hybrid dynamics  $\Sigma = (\mathcal{X}, f, \Delta, \phi)$ ,
- 2) an equilibrium point  $x_{\text{eq}} \in \mathcal{X}$  of  $f$ ,
- 3) a switching time  $\tau_0 \in \mathbb{R}$ , and
- 4) a vector of control parameters  $\mu_0 \in \mathbb{R}^k$

such that  $M_0(c_0) = 0$ , where  $c_0 = (x_{\text{eq}}, \tau_0, \mu_0) \in E_0$ , if  $c_0$  is a regular point of  $\mathcal{G}_0$ , then there exists a unique curve  $c : (-\delta, \delta) \rightarrow E_0$  of regular points contained in  $E_0$  that passes through  $c_0$  at  $c(0) = c_0$  for some  $\delta > 0$ .

**Algorithm 1** Detecting singular equilibrium gaits

**Require:** an interval  $[a, b] \subset \mathbb{R}$  and a step size  $h \in \mathbb{R}$ .

- 1: Define functions  $c_{\text{eq}}(t) = (x_{\text{eq}}, \tau_0 + t, \mu_0)$  and
- 2:  $\delta(t) = \det \left( \frac{\partial P}{\partial x_0}(c_{\text{eq}}(t)) - I_{2n} \right)$
- 3:  $N = \frac{b-a}{h}$
- 4: **for**  $i := 1..N$  **do**
- 5:    $t = a + i \times h$
- 6:   **if**  $\delta(t) \times \delta(t - h) \leq 0$  **then**
- 7:     Solve for  $\delta(t_0) = 0$  with  $t_0 \in [t - h, t]$
- 8:     Store  $c_{\text{eq}}(t_0)$  as a singular equilibrium point
- 9:     Store tangent vector  $\frac{dc_{\text{eq}}}{ds}(t_0)$  such that
- 10:     $J_0(c_{\text{eq}}(t_0)) \frac{dc_{\text{eq}}}{ds}(t_0) = 0$ ,  $\left\| \frac{dc_{\text{eq}}}{ds}(t_0) \right\| = 1$ , and
- 11:     $\frac{dc_{\text{eq}}}{ds}(t_0) \notin T_{c_{\text{eq}}(t_0)} E_0$ .
- 12:   **end if**
- 13: **end for**
- 14: **return** singular EGs and tangent vectors  $(c_{\text{eq}}(t_0), \frac{dc_{\text{eq}}}{ds}(t_0))$

*Proof.* See Appendix C.  $\square$

**Corollary 1.** If  $c_0 \in E_0$ , then  $\frac{\partial P}{\partial \tau}(c_0) = 0$  and  $J_0(c_0)$  has rank of at most  $2n + k$ . Furthermore, if  $c_0 \in E_0$  is a regular point of  $M_0$ , then the submatrix

$$\bar{J} = \begin{bmatrix} \frac{\partial P}{\partial x_0}(c_0) & \frac{\partial P}{\partial \mu}(c_0) \\ 0 & I_k \end{bmatrix} \in \mathbb{R}^{(2n+k) \times (2n+k)}$$

of the Jacobian  $J_0$  of Equation (8) has full rank  $2n + k$ .

The next proposition states that  $I(\tau)$  of Equation (7) can detect singular EGs in  $E_0$ .

**Proposition 2.** Assume there exists a path  $p : [0, 1] \rightarrow \mathcal{G}_0$  such that  $p(0) \in E_0$  and  $p(1) \in \mathcal{G}_0 - E_0$ . If  $p(0)$  is a regular point of  $M_0$ , then

- 1) the path  $p$  contains at least one singular equilibrium point  $p(s) \in E_0$ , and
- 2) for each singular equilibrium point  $p(s) \in E_0$  for  $s \in (0, 1)$ ,  $\det(\frac{\partial P}{\partial x_0}(p(s))) = 0$ .

*Proof.* See Appendix C.  $\square$

After identifying a singular EG using the indicator function, the next step is switching onto a branch of gaits in  $\mathcal{G}_0 - E_0$ . We can determine the correct branch for the case where the singular EG, say  $c_0$ , is isolated in  $E_0$  and its tangent space  $T_{c_0} \mathcal{G}_0$  is two dimensional.

**Proposition 3.** If  $c_0 \in E_0$  is an isolated singular point in  $E_0$  and  $\dim(T_{c_0} \mathcal{G}_0) = 2$ , then taking a step in the direction of the tangent vector in  $T_{c_0} \mathcal{G}_0$  orthogonal to the switching-time direction switches onto a branch of gaits in  $\mathcal{G}_0 - E_0$ .

*Proof.* See Appendix C.  $\square$

Given Propositions 1–3, we can automate the search for a singular EG along the switching-time axis (keeping the state and control constant) using Algorithm 1. Algorithm 1 finds simple roots of Equation (7) (i.e., if  $I(\tau) = 0$ , then  $\frac{dI}{d\tau}(\tau) \neq 0$ ) in a given interval by applying the intermediate value theorem to first bracket a root and then switching to a root-finding algorithm to accurately find the root. The step size  $h$  should

**Algorithm 2** Pseudo-arc length continuation method

**Require:**  $M : \mathbb{R}^{2n+k+1} \rightarrow \mathbb{R}^{2n+k}$  and step size  $h \in \mathbb{R}$ .

- 1: **function** CMSTEP( $c, \dot{c}, h$ )
- 2:   **Assume:**  $M(c) = 0$ ,  $\frac{\partial M}{\partial c}(c)\dot{c} = 0$ , and  $\|\dot{c}\| = 1$
- 3:   **Prediction Step:**
- 4:      $z = c + \dot{c}h$
- 5:   **Correction Step:**
- 6:     Solve for  $M(z) = 0$  and  $\dot{c}^T(z - c) = h$
- 7:     using Newton's method
- 8:     **return**  $z$
- 9: **end function**
- 10: **function** CMCURVE( $c_0, \frac{dc_0}{ds}, M$ )
- 11:   Set  $c[0] = c_0$  and  $\dot{c}[0] = \frac{dc_0}{ds}$ .
- 12:   **for**  $i := 1..N$  **do**
- 13:      $c[i] = \text{CMSTEP}(c[i-1], \dot{c}[i-1], h)$
- 14:     Set  $\dot{c}[i]$  such that  $\frac{\partial M}{\partial c}(c[i])\dot{c}[i] = 0$  and  $\|\dot{c}[i]\| = 1$
- 15:     **if**  $\dot{c}^T[i]\dot{c}[i-1] < 0$  **then**
- 16:        $h = -h$
- 17:     **end if**
- 18: **end for**
- 19: **return** the solution curve  $c$
- 20: **end function**

be chosen with care to avoid skipping over multiple roots in a given subinterval (we use  $3 \times 10^{-13}$ ). Alternative univariate root-finding algorithms can be found in [40]. In the end, all singular EGs detected using Algorithm 1, their corresponding tangent vector(s) that are orthogonal to the switching-time dimension, and the map  $M_0$  serve as inputs to the numerical continuation method (NCM) of the next section.

**Remark 4.** Conditions for when a singular EG is isolated can be found in [36]. In Proposition 3, we assume isolated singular points with  $\dim(T_{c_0} \mathcal{G}_0) = 2$  because it is the most common type of singular EG we encounter in practice.

*C. Tracing Branches with Numerical Continuation Methods*

Continuation methods are useful numerical tools for tracing the level set of a continuously differentiable function. While multi-dimensional continuation methods exist [20], [36], [41], we present an NCM for tracing one-dimensional manifolds (curves)  $c : \mathbb{R} \rightarrow \mathcal{G}$  in the  $(2n + k + 1)$ -dimensional state-time-control space  $\mathcal{S}$ . A curve in  $\mathcal{G}$  is implicitly defined such that every point on the curve  $c(s) \in \mathcal{G}$  satisfies

$$M(c(s)) = [P^T(c(s)), \Phi^T(c(s))]^T = 0, \quad (9)$$

where  $M : \mathcal{S} \rightarrow \mathbb{R}^{2n+k}$  is a continuously differentiable map,  $P$  is the periodicity map,  $\Phi(c) \in \mathbb{R}^k$  is a set of  $k$  auxiliary user-specified constraints to select a one-dimensional curve to trace in the  $(k + 1)$ -dimensional set  $\mathcal{G}$ , and  $s \in \mathbb{R}$  is the curve's arclength. The curve  $c$  is as smooth as the map  $M$  (Theorem 1).

For a user-defined map  $M$ , the function  $\Phi$  of Equation (9) defines the one-dimensional slice in  $\mathcal{S}$  that contains the curve  $c$ . The map  $\Phi_0$  of Equation (6) is an example of  $\Phi$ . In general, the map  $\Phi$  can contain any entry that can be computed as a function of  $c$ , including

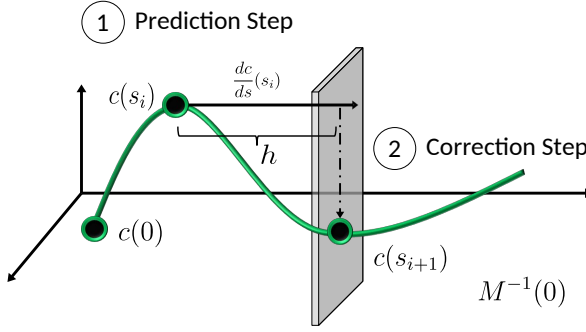


Fig. 3. An example iteration of the pseudo-arc length continuation method as outlined in Algorithm 2.

- 1) desired values for pre- or post-impact states,
- 2) gait properties like step length, walking speed, step incline, or minimum step height (which can be represented as an equality constraint using slack variables [42]), or
- 3) VHC boundary conditions, where, assuming  $a$  is the polynomial coefficient vector of the Bézier polynomials of Equation (1) and  $\mu = [\dots, a^T, \dots]^T$ , then  $x_0$  and  $a$  have to satisfy periodic boundary conditions of Equation (1) at  $t = 0$  and  $t = \tau$ .

Algorithm 2 describes the pseudo-arc length continuation method [36] for tracing a curve in  $\mathcal{G}$  using the map  $M$ . The core part of the algorithm is in CMSTEP; the function CMCURVE simply calls CMSTEP  $N$  times.

Geometrically, Algorithm 2 defines a hyperplane a distance  $h$  away from the current point  $c(s_i)$  on the curve where the search for the next point on the curve  $c(s_{i+1})$  takes place; the hyperplane is normal to the tangent  $\frac{dc}{ds}(s_i)$  at  $c(s_i)$ . The algorithm's prediction step (line 4 of the algorithm) selects a point on the plane as the initial guess using an Euler-like integration step and then a root-finding method iteratively refines the guess until the point is on the curve. Figure 3 illustrates this process.

In order to define the hyperplane, we can compute a tangent to the curve  $\frac{dc}{ds}(s)$  at  $c(s)$  by solving for  $\frac{\partial M}{\partial c}(c(s))\frac{dc}{ds}(s) = 0$  (line 14 of Algorithm 2). In other words, the tangent  $\frac{dc}{ds}(s)$  is in the null space of the Jacobian of the map  $M$

$$T_{c(s)}M^{-1}(0) = \text{Null}\left(\frac{\partial M}{\partial c}(c(s))\right), \quad (10)$$

where  $T_{c(s)}M^{-1}(0)$  is the tangent space of  $M^{-1}(0)$  at  $c(s)$ . An arclength parameterization of the curve leads to the constraint  $\|\frac{dc}{ds}(s)\| = 1$  (see [36]). If the point  $c(s)$  is a regular point of  $M$ , then  $\dim(T_{c(s)}M^{-1}(0)) = 1$  ( $= \dim(\mathcal{S}) - (2n + k)$  constraints).

Algorithm 3 is the projected Newton's method [43], [44], a root-finding algorithm for use in lines 6–7 of Algorithm 2. The projected Newton's method is a variant of Newton's method that imposes box constraints  $L \leq c \leq U$  on the values of  $c \in \mathcal{S}$ , where  $L, U \in \mathcal{S} \cup \{\pm\infty\}$  specify the lower- and upper-bounds of  $c$ , respectively, and the relational operators are applied elementwise. An application of the projected Newton's method is modeling inequality constraints, like the swing leg

---

### Algorithm 3 Projected Newton's method

---

**Require:**  $r : \mathcal{S} \rightarrow \mathbb{R}^m$ , where  $m \leq \dim(\mathcal{S})$ .

```

1: function PROJNEWT( $c, L, U$ )
2:    $z = c$ 
3:   repeat
4:     Compute Newton Step:
5:      $d = \frac{\partial r}{\partial c}(z)^\dagger r(z)$ , where  $[\cdot]^\dagger$  is the
6:     Moore-Penrose inverse
7:      $\Delta = z - d$ 
8:     Project onto Box Constraints:
9:     for  $1 \leq i \leq (2n + k + 1)$  do
10:      if  $\Delta[i] \leq L[i]$  then
11:        Set to lower bound:  $z[i] = L[i]$ 
12:      else if  $\Delta[i] \geq U[i]$  then
13:        Set to upper bound:  $z[i] = U[i]$ 
14:      else
15:        Take Newton step:  $z[i] = \Delta[i]$ 
16:      end if
17:    end for
18:   until a stopping criterion is met
19:   return  $z$ 
20: end function

```

---

of a biped staying above or on the walking surface, as equality constraints (see Section V for an example).

*Remark 5.* Part of the input to Algorithm 2 is a vector  $\frac{dc_0}{ds}$  tangent to the initial point  $c_0$ . If the manifold  $M^{-1}(0)$  is a one-dimensional differentiable manifold, then the tangent space is one-dimensional and there is no need to pass  $\frac{dc_0}{ds}$  as an argument; the algorithm can compute the tangent internally. However, we use NCMs to generate branches of connected components starting from a singular point, in which case we do need to specify the tangent vector as the null space has dimension greater than one [36]. If we do not specify the tangent at a singular point, the behavior of the algorithm is implementation dependent.

#### D. From Equilibria to One-Dimensional Sets of Walking Gaits

Given an EG  $c_{\text{eq}} \in E_0$ , Algorithm 4 constructs  $\mathcal{G}_{\text{mapped}}$  in a constant-control slice  $M_0(c) = 0$  in  $\mathcal{S}$ . For simplicity, we define  $\mathcal{G}_{\text{mapped}}$  as a two-dimensional array of gaits, but other data structures can be used. Most of the details of the algorithm are covered in Sections III-B and III-C (e.g., lines 2 and 8). In particular,  $N$  new gaits are added to  $\mathcal{G}_{\text{mapped}}$  when we successfully return from calls to Algorithm 2 (line 8). In the event that Algorithm 1 is not able to find isolated singular EGs, an error message is printed along with a plot of the indicator function  $I$  (lines 11–12). Further analysis of the plot provides potential directions for improving the model. We list an informal list of steps in Appendix B.

#### E. An Illustrative Example of the Basic Gait-Generation Approach Using the Compass-Gait Walker

We present an example of extending equilibria to periodic orbits for the passive compass-gait walker [14]. The compass-gait walker is a common two-link model. The model (Figure 4(a)) consists of two legs each with a point mass  $m$  and

**Algorithm 4** Constructing  $\mathcal{G}_{\text{mapped}}$  from equilibria

**Require:**  $c_{\text{eq}} \in E_0$ .

**1: Search for Singular Equilibrium Gaits:**

- 2: Call Algorithm 1 with a search interval of  $\tau \in [a, b]$ .
- 3: Store singular EGs and their tangent vectors in arrays
- 4:  $A$  and  $\dot{A}$ , respectively.

**5: Generate Curves in  $\mathcal{G} - E$ :**
**6: if**  $|A| > 0$  **then**
**7: for**  $i := 1..|A|$  **do**
**8:** $\mathcal{G}_{\text{mapped}}[i - 1][0..N] = \text{CMCURVE}(A[i], \dot{A}[i], M_0)$ 
**9: end for**
**10: else**
**11:**Print “No isolated singular equilibrium gaits found.”

**12:**Print plot of Indicator Function  $I(\tau)$  for  $\tau \in [a, b]$ .

**13: end if**
**14: return**  $\mathcal{G}_{\text{mapped}}$ 

length  $a + b$ . The biped also has a large point mass  $m_H$  at the hip. We use the same values for the physical parameters as in [14] with  $\frac{m_H}{m} = 2$ ,  $\frac{b}{a} = 1$ , and  $g = 9.81 \text{ m/s}^2$ . The state of the robot is  $x = [q_1, q_2, \dot{q}_1, \dot{q}_2]^T \in \mathbb{R}^4$ , representing the two leg angles and their velocities. With this minimal set of coordinates, we can directly compare our results to those in [14]. The angle of the walking surface  $\sigma \in \mathbb{R}$  is implicitly defined according to the position of the swing leg’s foot at  $t = 0$ :  $\sigma = \frac{1}{2}(q_1(0) + q_2(0))$ . The biped has no motors ( $n_u = 0$ ), no VHCs ( $n_v = 0$ ), and two PHCs ( $n_p = 2$ ) representing the no-slip contact conditions between the stance foot and the ground.

After using this data to derive the biped’s hybrid dynamics, the goal is to find period-one walking gaits in a five-dimensional state-time space  $\mathcal{S}$ . A point  $c \in \mathcal{S}$  consists of the pair  $(x_0, \tau)$ , where  $x_0 \in \mathcal{X}$  is a pre-impact state and  $\tau \in \mathbb{R}$  is a switching time (in seconds). There are no control parameters  $\mu$  ( $k = 0$ ). Given the five parameters that define  $\mathcal{S}$  and the four periodicity constraints of the periodicity map  $P$ , we expect to find one-dimensional manifolds of gaits in  $\mathcal{S}$ . The search for a walking gait starting on a manifold of equilibrium gaits (EGs) is a two-step process:

- 1) Identify a subset of EGs of interest in  $E \subset \mathcal{G}$ ,
- 2) Choose a  $c_{\text{eq}} \in E$  and call Algorithm 4, which
  - a) calls Algorithm 1 to find all singular EGs in a closed interval of switching times  $\tau \in [a, b] \subset \mathbb{R}$  where  $0 \leq a < b$ , then
  - b) calls Algorithm 2 with the map  $M_0 = P$ , a singular EG  $c_{\text{eq}}$ , and the correct tangent vector  $\frac{dc_{\text{eq}}}{ds}(s) \in T_{c_{\text{eq}}}P^{-1}(0)$ .

The first step for the compass gait is straightforward. The biped’s state space  $\mathcal{X}$  has four one-stance-foot equilibrium points (EGs), but only two EGs in  $\mathcal{X}$  correspond to fixed points of  $\mathcal{G}$  because of the flip operator. These are  $x_{\text{eq}} = [0, 0, 0, 0]^T$  (standing on a surface) and  $x_{\text{eq}}^\pi = [\pi, \pi, 0, 0]^T$  (hanging below a surface), as shown in Figure 4(b)–(c). These points define the set of equilibria  $E \subset \mathcal{G}$ , where  $E = E_0 \cup E_\pi$ ,  $E_0 = \{c_{\text{eq}} \in \mathbb{R}^5 : [0, 0, 0, 0, \tau]^T\}$ , and  $E_\pi = \{c_{\text{eq}} \in \mathbb{R}^5 : [\pi, \pi, 0, 0, \tau]^T\}$ . We start our search using the equilibrium  $x_{\text{eq}}$ , which gives rise

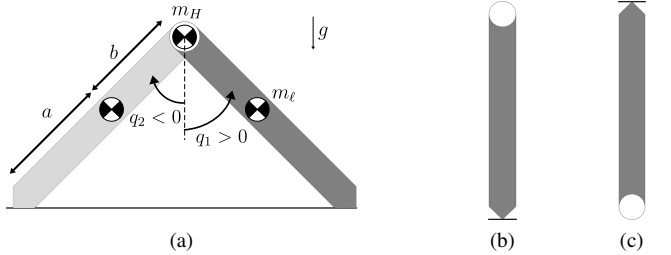


Fig. 4. The compass-gait model and two equilibrium points in  $\mathcal{G}$ . The legs in the model have the same physical parameters  $a$ ,  $b$ , and  $m_H$ .

to nearby walking gaits. If we had started with  $x_{\text{eq}}^\pi$ , we would find nearby (overhand) brachiating gaits.

Algorithm 4 performs the next step in two parts. The algorithm first calls Algorithm 1 to find roots of the indicator function  $I(\tau)$  of Equation (7) over the interval  $\tau \in [0, 1]$ . The roots correspond to the singular EGs of Figure 5 at  $\tau = 0.62$  s and  $\tau = 0.68$  s, respectively (red dots with black circles).

At these singular EGs, there are two tangent vectors in the null space of  $J(c) = \frac{\partial P}{\partial c}(c)$  of Equation (3). Choosing an orthonormal basis, the tangent vector that leads to the branch of walking gaits is orthogonal to the switching-time dimension in  $\mathcal{S}$ . Setting  $e_0 = [0, 0, 0, 0, 1]^T$ , then an orthonormal basis for the null space evaluated at  $J(x_{\text{eq}}, 0.62)$  is  $\{e_0, [0.13, -0.12, 0.72, 0.67, 0]^T\}$  and at  $J(x_{\text{eq}}, 0.68)$  is  $\{e_0, [0.13, -0.13, 0.69, 0.69, 0]^T\}$ . The desired tangent in each case is not  $e_0$  (which points along the switching-time dimension), as shown in the proof of Proposition 3.

Algorithm 4 then calls the pseudo-arc length continuation method of Algorithm 2 starting from each of the singular EGs identified in the previous step. Figure 5 shows the resulting set of gaits  $\mathcal{G}_{\text{mapped}}$  and animations of a selection of gaits from  $\mathcal{G}_{\text{mapped}}$ , respectively. The path-connected set of gaits in Figure 5(a) reflects the description given earlier in Section III-A of the connected components of EGs. In this plot, we have seven different 1D manifolds of gaits (red and green curves) joined together at two singular EGs (black dots). In particular,  $(x_{\text{eq}}, 0)$  is part of a set of equilibrium branches of gaits with zero net displacement (red line) such that  $(x_{\text{eq}}, \tau)$  is a point on these branches for all  $\tau$ . The red line of EGs intersects with two green branches of walking gaits. The points of intersection at  $\tau = 0.62$  s and  $\tau = 0.68$  s for the compass gait correspond to the start of the “short” and “long” solution branches of walking gaits as reported in [14]. The (symmetric) green branches that extend from each singular point contain gaits that are mirror images of each other, i.e., if one branch has state  $x_0$ , the other branch has state  $-x_0$ ; the sign indicates whether the gait walks downhill to the left or right of its initial stance.

In Figure 5(b)–(g), we see the existence of gaits in  $\mathcal{G}_{\text{mapped}}$  over a range of slopes that include walking and overhand brachiating gaits. Each of the gaits in Figure 5(b)–(g) can be continuously deformed into each other and are part of the same connected component of the EG  $(x_{\text{eq}}, 0)$  depicted in Figure 4(b).

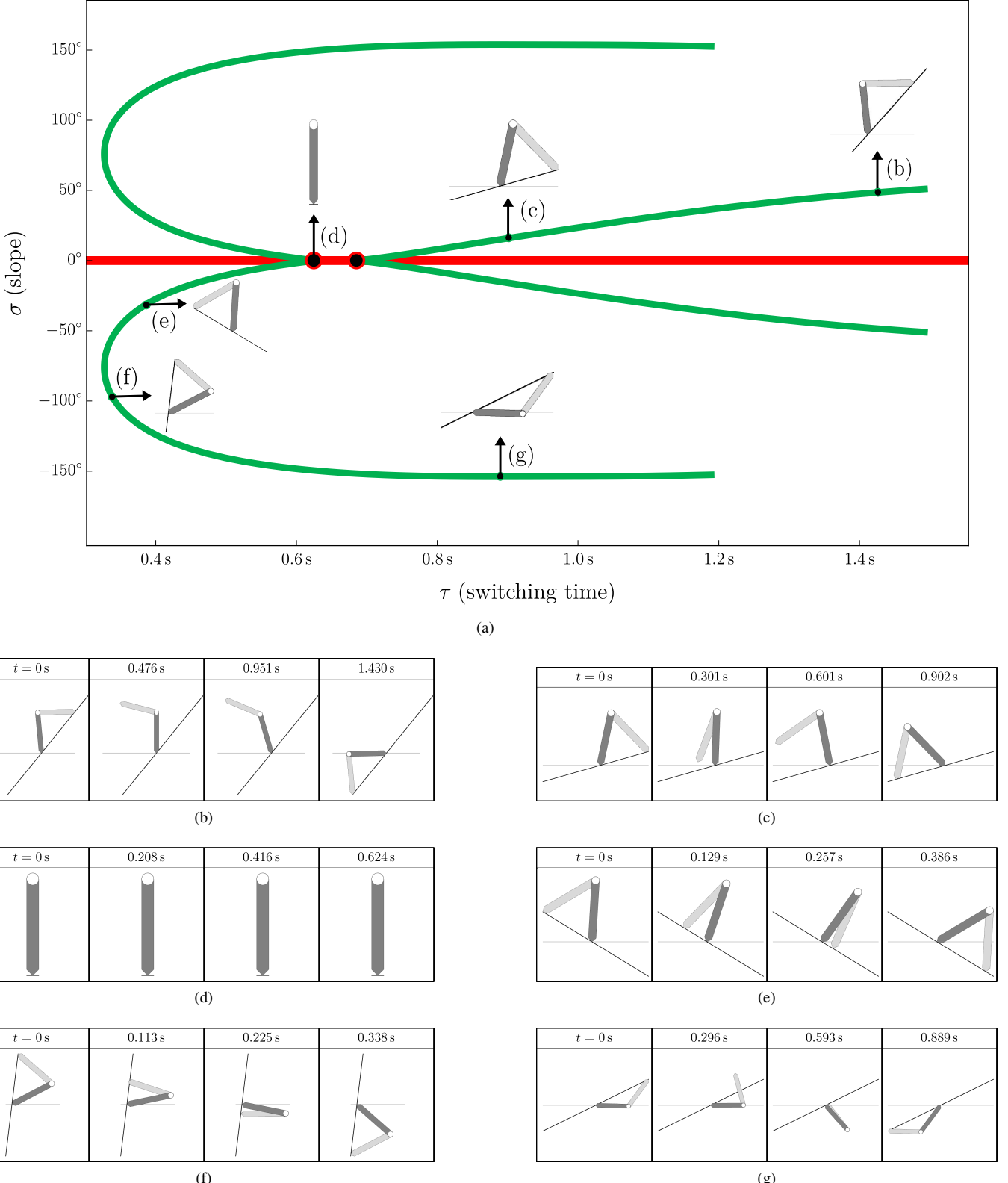


Fig. 5. (a) A continuous set of unactuated periodic motions  $\mathcal{G}_{\text{mapped}}$  that satisfy the compass gait's hybrid dynamics as points in a parameter space  $\mathcal{S}$  projected onto a slope-switching-time ( $\sigma$ - $\tau$ ) plane (red and green curves); the slope  $\sigma$  is the biped's walking surface. The plot consists of four 1D manifolds of walking and brachiating gaits (green curves), three equilibrium branches (red curves), and two singular equilibrium gaits (red dots with black circles). Specifically, each of the two leftmost green curves are linear interpolations of 250 gaits computed with Algorithm 4 (the maximum number of gaits we have Algorithm 4 compute), the two rightmost green curves consist of the first 113 points we computed on each branch, and the red line is added after the fact to represent the equilibrium branches. The callout labels in the plot correspond to the animated trajectories in (b)–(g); the images in the plot are the pre-impact configurations of the biped at  $t = 0$ . (b)–(g) The motion of the gaits depicted in (a) with respect to (absolute) time  $t \geq 0$ . Gaits (b), (c), (f), and (g) locomote from right to left and (e) goes from left to right. Because of the biped's symmetry, every gait in (a) has a mirrored version of itself about the  $\tau$  axis. In other words, trajectories in (b)–(g) that locomote on a slope  $\sigma$  have mirrored trajectories that walk or brachiate downhill on a slope of  $-\sigma$ .

#### IV. EXTENSIONS TO THE APPROACH

In the previous section, we focused on constant-control slices in  $\mathcal{G}$ . We now present extensions to the approach for

- 1) constructing multi-dimensional manifolds in  $\mathcal{G}_{\text{mapped}}$  from EGs (Section IV-A), and
- 2) searching the manifolds of  $\mathcal{G}$  for gaits with desired properties, for example, specific walking speeds or values for  $x_0$ ,  $\tau$ , or  $\mu$  (Section IV-B).

These extensions expand our work beyond passive dynamic walkers. In particular, for biped models that cannot balance on one foot, EGs for use as input to Algorithm 4 may not exist or may be difficult to find. In order to handle these types of models, we add control parameters that continuously modify the physical parameters of the biped model. For example, in Section V, we introduce a control parameter  $\omega \in [0, 1]$  that parameterizes a family of MARLO biped models with different hip widths and center of mass positions such that  $\omega = 0$  corresponds to a planarized version of MARLO and  $\omega = 1$  corresponds to the 3D model used in [22]. The purpose of parameters such as  $\omega$  is to start with a model that has a simple set of EGs that can be used as input to Algorithm 4 (e.g., the EGs for MARLO at  $\omega = 0$ ) and to then eventually connect these gaits to a family of walking gaits of the desired biped model (for MARLO, walking gaits with control parameter  $\omega = 1$ ). Given that the number of control parameters  $k$  will necessarily be greater than zero, this motivates the use of algorithms that can search higher-dimensional manifolds for desired gaits.

##### A. Constructing Multi-Dimensional Manifolds

Algorithm 5 is an example of a higher-dimensional continuation method. It uses the map  $M_0$  and a collection of  $k$  additional maps  $M_1, \dots, M_i, \dots, M_k$  such that the level set  $M_i(c) = 0$  defines a constant slice in  $\mathcal{S}$  where the switching time and all but the  $i^{\text{th}}$  control parameter are fixed:

$$\begin{aligned} M_i(c) &= [P^T(c), \Phi_i^T(c)]^T \\ \Phi_i(c) &= [\tau - t, \mu_1 - v_1, \dots, \mu_{i-1} - v_{i-1}, \\ &\quad \mu_{i+1} - v_{i+1}, \dots, \mu_k - v_k]^T, \end{aligned} \quad (11)$$

where  $c = (x_0, \tau, \mu) \in \mathcal{S}$  is the input;  $1 \leq i \leq k$  is the  $i^{\text{th}}$  control parameter in  $\mu$  that varies throughout the continuation;  $P$  is the periodicity map;  $\Phi_i : \mathcal{S} \rightarrow \mathbb{R}^k$  defines the slice in  $\mathcal{S}$ ;  $t \in \mathbb{R}$  is a switching time; and  $\mu_j$  and  $v_j$  are the  $j^{\text{th}}$  element ( $j \in [1, k] - \{i\} \subset \mathbb{N}$ ) of the control parameter vectors  $\mu$  and  $v$ , respectively, such that  $\mu_j$  is held fixed at the value  $v_j$ .

The algorithm generalizes Algorithm 4 by using  $M_0$  and the  $k$  maps of Equation (11) to recursively construct a  $(k+1)$ -dimensional manifold. The algorithm recurses on the dimension  $d$  ( $0 \leq d \leq k+1$ ) of the manifold. The base case of  $d = 0$  returns a singular EG, which is the seed value for constructing a curve for the case of  $d = 1$ . The recursive step generates gaits for a  $d$ -dimensional manifold using the gaits on a  $(d-1)$ -dimensional submanifold as seed values.

While this algorithm allows for the control space to vary throughout the continuation, it becomes impractical for large

---

##### Algorithm 5 Constructing multi-dimensional manifolds

**Require:** singular equilibrium gait  $c_{\text{eq}} \in E_0$ .

```

1: function MULTI-DIM( $d$ )
2:   if  $d = 0$  then
3:     return  $\{c_{\text{eq}}\}$ 
4:   else
5:      $\mathcal{G}_{d-1} = \text{multi-dim}(d-1)$ 
6:     return  $\bigcup_{g \in \mathcal{G}_{d-1}} \text{CMCURVE}(g, \frac{dg}{ds}, M_{d-1})$ 
7:   end if
8: end function

```

---

*k.* The algorithm is a brute-force approach to searching higher-dimensional manifolds for desired gaits as we have to continue to run the algorithm until it happens to come across a gait we are interested in.

##### B. Finding Desired Gaits Using the Global Homotopy Map

In this section, we give an algorithm for searching  $(k+1)$ -dimensional gait manifolds for gaits with desired properties, such as gaits for walking on flat ground. A core part of the algorithm is the use of the global homotopy map (GHM) [36], [45] to find these gaits. The GHM continuously deforms gaits found using our previous map  $M_0$  into gaits that satisfy the periodicity constraints of the map  $P$ , and up to  $k$  additional constraints, by varying all parameters in  $\mathcal{S}$  at the same time. The GHM  $G : \mathcal{S} \rightarrow \mathbb{R}^{n_h}$  is

$$\begin{aligned} G(c) &= H(c) - p H(a), \quad a \in \mathcal{G}_{\text{mapped}} - H^{-1}(0), \\ p(c) &= (H^T(a)H(c))/(H^T(a)H(a)). \end{aligned} \quad (12)$$

The map  $H : \mathcal{S} \rightarrow \mathbb{R}^{n_h}$  ( $n_h \leq k$ ) is similar to  $\Phi$  of Equation (9) with the exception that  $H$  can specify fewer than  $k$  constraints. The gait  $a \in \mathcal{G}_{\text{mapped}} - H^{-1}(0)$  serves as a template motion that we attempt to continuously deform into a desired gait—a to-be-determined point  $c \in \mathcal{S}$  satisfying  $H(c) = 0$ . The parameter  $p(c) \in [0, 1]$  is the homotopy parameter that continuously deforms the reference gait  $a$  into a gait on the  $H(c) = 0$  slice in  $\mathcal{S}$ . Two important properties of the homotopy parameter are the following:

- 1) for  $c = a$ , we have  $p(a) = 1$ , which makes  $a$  a trivial root of  $G$  (i.e.,  $G(a) = H(a) - p(a)H(a) = H(a) - H(a) = 0$ ), and,
- 2) for points  $c_0 \in H^{-1}(0)$ , we have  $p(c_0) = 0$  and  $G(c_0) = H(c_0) - p(c_0)H(a) = H(c_0) = 0$  thus making  $c_0$  roots of  $p$  and  $G$  as well.

The GHM is a type of auxiliary function that is meant to be used to query the gait space. As an illustrative example, let  $\sigma(c) \in \mathbb{R}$  compute the incline of a planar biped's walking surface and  $\nu(c) \in \mathbb{R}$  compute the biped's average walking velocity, then the structure of the query is: Given the manifold in  $\mathcal{G}$  that contains the gait  $a$ , find a gait  $c_0$  that walks on flat ground ( $\sigma(c_0) = 0$ ) at 0.7 m/s. The constraint function  $H = [\sigma(c), \nu(c) - 0.7]^T = 0$  is used to encode the query as a set of equality constraints. We now integrate the GHM map into the rest of our framework.

Let  $n_G = 2n + n_h$  be the number of total constraints and  $k_G = k + 1 - n_h$  be the number of expected freedoms (as

**Algorithm 6** A modified continuation method for use with the map  $M_a$  of Equation (13)

---

**Require:**  $M_a : \mathbb{R}^{2n+k+1} \rightarrow \mathbb{R}^{n_G}$ ,  $a \in M_a^{-1}(0)$ ,  $\alpha \in \mathbb{R}$ , and  $\beta \in \mathbb{R}$ .

- 1: **function** GHM( $c$ )
- 2:   **Assume:**  $M_a(c) = 0$
- 3:   Define merit function:  $f(x) = \frac{1}{2}p(x)^2$ .
- 4:   **Newton Step:**
- 5:   Solve for  $\frac{\partial c}{\partial s}$  such that  $\frac{\partial M_a}{\partial c}(c)\frac{\partial c}{\partial s} = 0$  and
- 6:    $\frac{\partial c^T}{\partial s}\frac{\partial c}{\partial s} = I_{k_G}$ , where  $I_{k_G}$  is a  $k_G \times k_G$  identity matrix.
- 7:    $\Delta s = -\left[\frac{\partial p^T}{\partial c}(c)\frac{\partial c}{\partial s}\right]^\dagger p(c)$
- 8:   **Perform Line Search:**
- 9:   Set  $m = 0$  and  $\dot{c} = \frac{\partial c}{\partial s}\Delta s$ .
- 10:   **repeat**
- 11:    Set  $\lambda = \beta^m$ ,  $m = m + 1$ , and  $h = \lambda\Delta s$
- 12:     $z = \text{CMSTEP}(c, \dot{c}, h)$  (see Algorithm 2)
- 13:    **until**  $f(z) - f(c) \leq -\alpha\lambda\frac{\partial f^T}{\partial s}(c, \dot{c})\Delta s$
- 14:   **return**  $z$
- 15: **end function**
- 16: **Generate Curve:**
- 17: Set  $c[0] = a$ .
- 18: **for**  $i := 1..N$  **do**
- 19:    $c[i] = \text{GHM}(c[i-1])$
- 20: **end for**
- 21: **return** the solution curve  $c$

---

singularities on a connected component can cause the number of freedoms to increase). Given the GHM, define the map  $M_a : \mathcal{G} \rightarrow \mathbb{R}^{n_G}$  as

$$M_a(c) = [P^T(c), G^T(c)]^T. \quad (13)$$

The space  $M_a^{-1}(0)$  is comprised of  $k_G$ -dimensional manifolds in  $\mathcal{G}$ . The goal is to find a path from a known gait  $a \in \mathcal{G}_{\text{mapped}}$  to a gait  $c \in \mathcal{G}$  such that  $H(c) = 0$ . From Equation (12), this is equivalent to finding a root of  $p$ . In order to find a root of  $p$ , we modify Algorithm 2 so that we simultaneously generate  $\mathcal{G}_{\text{mapped}}$  and search for a gait in  $\mathcal{G}$  that is a root of  $p$ . The modified algorithm is summarized in Algorithm 6.

**Proposition 4.** Given a point  $a \in \mathcal{G}_{\text{mapped}} - H^{-1}(0)$  sufficiently close to a root of  $p$  and the map  $M_a$ , if, at every iteration  $i$  ( $1 \leq i \leq N$ ) of Algorithm 6, the tangent vector  $\frac{dc}{ds}(s_i) \in T_{c(s_i)}M_a^{-1}(0)$  is chosen such that

$$\frac{dc}{ds}(s_i) = -\frac{\partial c}{\partial s}(s_i) \left[ \frac{\partial p^T}{\partial c}(c(s_i)) \frac{\partial c}{\partial s}(s_i) \right]^\dagger p(c(s_i)),$$

where  $[\cdot]^\dagger$  is the Moore-Penrose inverse and  $\frac{\partial c}{\partial s}(s_i) \in \mathbb{R}^{(2n+k+1) \times k_G}$  is a matrix whose  $k_G$  columns are basis vectors for  $T_c M_a^{-1}(0)$  at  $c \in M_a^{-1}(0)$ , then tracing the vector field  $\frac{dc}{ds}(s_i)$  starting from a simultaneously defines a one-dimensional curve of fixed points  $c(s_i) \in M_a^{-1}(0) \subseteq \mathcal{G}$  and a sequence of Newton iterates that converges to a root of  $p$ .

*Proof.* We prove the proposition in two steps. First, we derive the direction of a Newton step  $\Delta s \in \mathbb{R}^{k_G}$  for numerically solving  $p(c(s)) = 0$ , where  $s \in \mathbb{R}^{k_G}$  is some parameterization

of the manifold  $M_a(c(s)) = 0$ . We then project  $\Delta s$  onto the tangent space  $T_{c(s)}M_a^{-1}(0)$  using  $\frac{\partial c}{\partial s}(s)$ .

As the system of equations  $p(c(s)) = 0$  is not square, we use the Moore-Penrose inverse to define a Newton step  $\Delta s$  [46] from a Taylor approximation of  $p$  about a root; that is from  $p(c(s + \Delta s)) \approx p(c(s)) + \frac{\partial p^T}{\partial c}(s)\frac{\partial c}{\partial s}(s)\Delta s = 0$ , we get  $\Delta s = -\left[\frac{\partial p^T}{\partial c}(c(s))\frac{\partial c}{\partial s}(s)\right]^\dagger p(c(s))$ .

At iteration  $i$  of Algorithm 6, we project the Newton step onto the tangent space  $T_{c(s_i)}M_a^{-1}(0)$  at  $c(s_i) \in M_a^{-1}(0)$ , which yields the tangent vector

$$\frac{dc}{ds}(s_i) = -\frac{\partial c}{\partial s}(s_i) \underbrace{\left[ \frac{\partial p^T}{\partial c}(c(s_i)) \frac{\partial c}{\partial s}(s_i) \right]^\dagger p(c(s_i))}_{-\Delta s}.$$

This choice leads to a curve being traced in  $M_a^{-1}(0)$  with points on the curve that converge to a root of  $p$ .  $\square$

Algorithm 6 contains the function GHM for computing a new point  $z \in M_a^{-1}(0)$  from  $c \in M_a^{-1}(0)$  based on Proposition 4. In order to ensure that we are making progress towards a root, we take a step of magnitude  $h$  in the direction of  $\frac{dc}{ds}(s) = \frac{\partial c}{\partial s}(s)\Delta s$  based on an Armijo line search [44] using the merit function  $f(c(s)) = \frac{1}{2}p(c(s))^2$ . This leads to an adaptive step size strategy for  $h$ . Typical values used for  $\alpha$  and  $\beta$  in Algorithm 6 are  $10^{-4}$  and 0.5, respectively [44].

**Remark 6.** Algorithm 6 differs from Algorithms 2–5 in that the input map  $M_a$  does not have to define one-dimensional level sets (e.g.,  $M_0(c) = 0$  of Algorithm 4). Instead, Algorithm 6 selects a descent direction in a high-dimensional tangent space using a merit function similar to many optimization-based methods [31], [42].

**Remark 7.** For biped models with sufficient control authority, we can seed the gait  $a$  of Algorithm 6 with an EG that is a regular point of  $P$ . A biped has sufficient control authority if any regular EG has a local neighborhood of gaits in  $\mathcal{G} - E$  on the  $(k+1)$ -dimensional manifold it is on. If not, we would have to search for singular EGs as outlined in Section III-B.

**Remark 8.** In Section IV, we discussed using the control parameters to define a family of 2D and 3D biped models. An important application of the GHM is taking the parameterized model and, for example, continuously deforming a gait for a planar version of the model (where the EGs are trivial to specify) into gaits for a 3D version of the biped model.

## V. EXAMPLES

We have applied our framework to several bipeds taken from the literature (Figure 6) to confirm its wide applicability. The biped models range from planar passive dynamic walkers to high-degree-of-freedom actuated 3D humanoids. The details of these bipeds can be found in the Multimedia Material. In this section, we expand on using equilibria to generate actuated gaits for the compass gait [14], MARLO [25] (Figure 6(f)), and Atlas [51] (Figure 6(g)) bipeds.

All bipeds are modeled as kinematic trees with floating bases attached to their pelvis [52]. If the biped is planar the

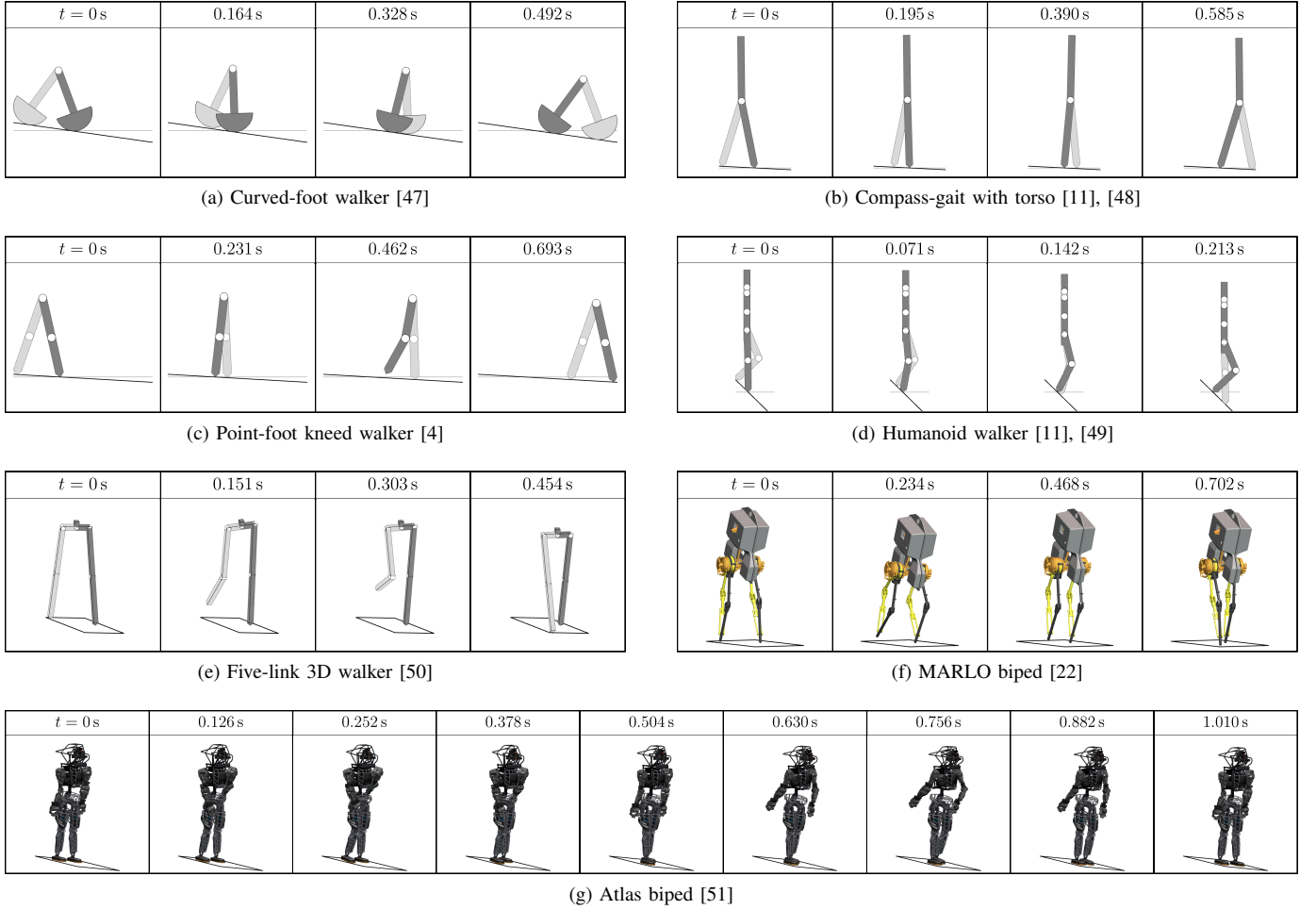


Fig. 6. Example period-one gaits for various biped walkers. The dots are joint centers. Gaits pictured in (a)-(d) are walking passively downhill and (e)-(g) are powered gaits that are subject to virtual holonomic constraints; (e)-(f) are walking on flat ground; (g) is walking downhill.

floating base has three configuration variables, otherwise the floating base has six configuration variables. Unless otherwise noted,

- 1) physical quantities are measured in SI units (i.e., meters, kilograms, seconds),
- 2) the gaits reported in this paper have a normed error between two consecutive pre-impact states  $x_0 = (q, \dot{q})$  of less than  $10^{-8}$  (with  $q$  having units of radians and  $\dot{q}$  radians per second),
- 3) the search window for singular equilibrium gaits for Algorithm 1 is  $\tau \in [0.1, 1]$  divided into 100 steps,
- 4) the step size  $h$  of the NCM of Algorithm 2 is  $\pm \frac{1}{20}$  in order to trace both sides of a curve. We attempt to generate  $N = 250$  gaits per function call,
- 5) the  $x$ ,  $y$ , and  $z$  axes of the world and local frames of our 3D biped models are labeled with blue, red, and green arrows, respectively, and
- 6) gaits are computed on a 2.7 GHz Intel Core i7-4800MQ CPU laptop running 64-bit Ubuntu 18.04 LTS.

The Multimedia Material contains an implementation of our framework as a Mathematica library. Given model-specific information, like the biped's PHCs and VHCs, the code is capable of finding entire families of walking gaits using only

equilibria of the biped models. The code computes items like the map  $P$ , the flow  $\varphi$ , and their respective derivatives from the model.

#### A. Extending Passive Gaits into a Family of Actuated Gaits

If we add a motor at the hip joint of the compass-gait robot as described in Section III-E, the state-time space  $\mathcal{S}$  can be augmented with control dimensions. In general, increasing the dimension of  $\mathcal{S}$  will also increase the dimension of  $\mathcal{G}$ . The original  $\mathcal{G}$  is just the  $\mu = 0$  slice of the extended  $\mathcal{G}$ .

We use the motor to drive leg 2 relative to leg 1 with the torque  $u_0(t) = \mu_0 \sin(\omega t)$  [53], where the amplitude  $\mu_0 \in \mathbb{R}$  is a control parameter. The angular frequency is fixed at  $\omega = 2\pi$  to keep this example low dimensional. The control dimension is one ( $k = 1$ ) and we have added an actuator ( $n_u = 1$ ) to the model. Design parameters could also be defined. For example, a parameter defining the curvature of the feet [47] or position of the center of mass [13] could be added. In this example, however, we only add the control parameter  $\mu_0$ . Figure 7(a) shows an actuated gait in the extended gait space. The value of  $\mu_0$  for this step is  $-5.34 \text{ N m/(kg m}^2\text{)}$  and becomes  $5.34 \text{ N m/(kg m}^2\text{)}$  at the start of the next step. As

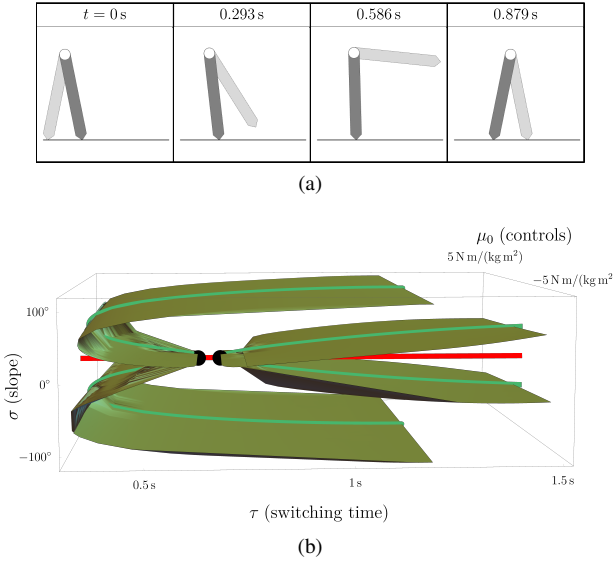


Fig. 7. (a) An actuated gait of the compass-gait walker walking on flat ground, where  $u(t) = \mu_0 \sin(\omega t)$  with  $\omega = 2\pi$ . For this step,  $\mu_0 = -5.34 \text{ N m}/(\text{kg m}^2)$ . At the start of the next step,  $\mu_0 = 5.34 \text{ N m}/(\text{kg m}^2)$ . (b) A connected component of the compass-gait walker in a higher-dimensional state-time-control space (see Figure 2 for legend). The curves of passive gaits in Figure 5 are slices of this space where  $\mu_0 = 0$  (green and red curves).

masses and lengths are scaled in the model, this corresponds to a maximum output torque of about  $\frac{\mu_0}{4} = 1.34 \text{ N m}$ .

In this six-dimensional state-time-control space  $\mathcal{S}$  consisting of points  $(x_0, \tau, \mu_0)$ , we have two-dimensional gait manifolds (the six parameters minus the four periodicity constraints). The passive gaits of the previous section are now a slice of this higher-dimensional gait space  $\mathcal{G} \subset \mathbb{R}^6$ , where the control parameter  $\mu_0$  is zero (Figure 7(b)).

Algorithm 5 is used to construct the surface of Figure 7(b). The algorithm first uses the map  $M_0$  of Section III-B to generate a set of passive gaits using the seed values  $(x_{\text{eq}}, 0.62, 0)$  and  $(x_{\text{eq}}, 0.68, 0)$  (i.e., the singular points of the original  $\mathcal{G}$  space mapped to the extended  $\mathcal{G}$  space). Our Mathematica implementation of the algorithm took 7.2 minutes to compute the 828 passive gaits in Figure 7(b). Algorithm 5 then uses every gait found in  $M_0^{-1}(0)$  as seed values to Algorithm 2 using the map  $M_1 : \mathcal{S} \rightarrow \mathbb{R}^{2n+k}$  of Equation (11), which holds  $\tau$  constant and allows  $\mu_0$  to vary during the continuation. The library took 1.8 hours to compute the 18,400 actuated gaits in Figure 7(b).

This higher-dimensional example shows that we can grow  $\mathcal{G}_{\text{mapped}}$  from an EG to a set of passive gaits to an even larger set of actuated gaits by adding extra control parameters to the state-time-control space  $\mathcal{S}$ . We use this notion of growing a manifold from lower-dimensional slices for our 3D bipeds as well. In this case, we generate gaits for a planar or simplified 3D version of the biped and use these walking gaits to generate gaits for the full 3D model.

### B. Generating Gaits for a Flat-footed Walking Biped with Arms

We have tested our technique on a simulation of a version of Boston Dynamics' Atlas, a 3D flat-footed walking biped (Fig-

ure 8(a)). The use of flat-footed walking constraints is inspired by the reduced models of [6], [32], which only consider the legs of Atlas as their biped model. In this example, we generate gaits for a biped with fewer actuators than internal degrees of freedoms ( $n_u < n-6$ ). This example demonstrates that we can generate gaits for complicated underactuated bipeds subject to VHCs.

The model we use for Atlas is from a DARPA Robotics Challenge “.cfg” file available online [54]. This source file generates the biped’s URDF file for use in ROS and Gazebo. We use the full model with 3D dynamics and a 6D floating base at the pelvis. The only changes to the model are

- 1) zeroing the  $y$  position of the center of mass of two links (see Multimedia Material) to make the model physically symmetric (Assumption A1), and
- 2) defining the biped’s home position with the arms pointing downwards (Figure 8(a)), so that  $x_{\text{eq}} = 0 \in \mathcal{X}$  can be an equilibrium point.

In the end, our model of Atlas has 34 degrees of freedom when unconstrained (Figure 8(a)). The model has 15 VHCs and 15 actuators. However, the VHCs and actuators are not all active during a step. When a VHC is not active, an actuator is considered off and the joint attached to the inactive actuator is unactuated during the step.

During a step, the biped walks in its sagittal plane and is subject to six PHCs that fix the stance foot to the ground ( $n_p = 6$ ), 13 active VHCs ( $n_v = 13$ ), and 13 active actuators to enforce the VHCs ( $n_u = 13$ ). Atlas’ remaining 15 internal joints that are not subject to VHCs as well as the 6 joints of the floating base are unactuated.

The set of active VHCs depends on whether the left or right leg is the stance leg. At the post-impact time  $t = 0^+$ , we assume the left leg is the stance leg. The configurations and velocities of the joints about the  $x$  and  $z$  axes at the hips,  $y$  axis at the neck,  $x$  and  $y$  axes at the ankles,  $y$  axis at the right elbow, and  $x$  axis at the wrists are subject to VHCs that force the joints to track third-order Bézier polynomials. The configuration of the left knee joint is subject to the final VHC that keeps the relative knee angle locked at zero degrees throughout the motion post-impact. Further details, like the active set of VHCs when the right leg is the stance leg, can be found in the Multimedia Material.

From this data, the biped’s pre-impact state is  $x_0 \in \mathcal{X} \subset \mathbb{R}^{68}$  ( $n = 34$ ). In our code, we use the PHCs and VHCs to reduce the number of independent states in  $x_0$  down to 33 state variables and define  $x_0$  as a function of a reduced state vector  $\bar{x}_0 \in \mathbb{R}^{33}$  such that  $x_0 = x_0(\bar{x}_0)$ .

In addition to the states, we define two control parameters  $\omega_1, \omega_2 \in [0, 1]$ , making  $\mu = [\omega_1, \omega_2]^T \in \mathcal{M}$ . These dimensionless control parameters modify the biped’s physical parameters to create a 3D model that can balance on one foot at  $x_0 = 0$ . The parameter  $\omega_1$  affects every link’s center of mass position and relative distance from the pelvis along the link’s  $x$  axis (i.e., if the distance of link  $i$  from the pelvis along the  $x$  axis was  $\delta x_i$ , then the model would contain the product  $\omega_1 \delta x_i$ ). The parameter  $\omega_2$  affects the center of mass position along the  $y$  axis of every link’s center of mass. When both parameters are zero, they, along with the active

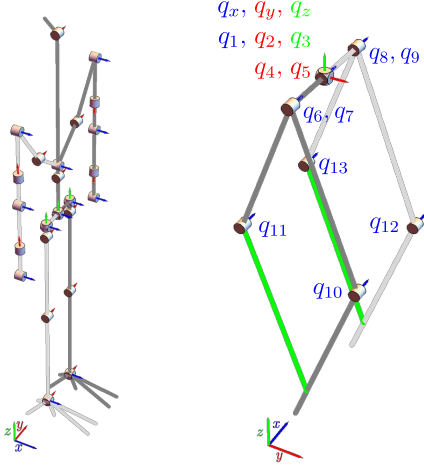


Fig. 8. Mechanical structure and coordinates for the models of Atlas (left) and MARLO (right). The light gray links are on the “right-side” of the bipeds, the cylinders are joints, the arrows emanating from the cylinders are the (positive) rotation axes, and the  $x$ - $y$ - $z$  frames are world frames. In addition, MARLO has joint centers that overlap and are not visible, and green links to emphasize the leg’s four-bar structure.

VHCs, eliminate the non-zero moments about the joints due to the gravity vector making the configuration depicted in Figure 8(a) an equilibrium for the model. A value of one for each parameter gives the original biped model.

In total, the biped has a 71-dimensional state-time-control space  $\mathcal{S}$  (68 states, 2 control parameters, and 1 switching time). We define  $M_0$  of Equation (6) so that  $\omega_1 = \omega_2 = 0$  throughout the continuation making  $\mu_0 = 0$  in  $M_0$ . At these fixed values of the control parameters, we generate gaits for Atlas using the same process as we did with the compass gait.

For the parameterized model at  $\omega_1 = \omega_2 = 0$ , a singular EG found in the constant-control slice occurs at  $\tau = 0.396$  s. Algorithm 4 performs a NCM using the map  $M_0$  starting at the singular EG at  $\tau = 0.396$  s. Our Mathematica code took 1.5 hours to compute 250 gaits. We then apply Algorithm 6 to find a gait with  $\omega_1 = \omega_2 = 1$ . The library took 1.8 hours to find a gait with the desired values and computed 48 gaits in the process. The desired gait from this continuation is shown in Figure 6(g). The biped is shown taking two steps.

### C. Incorporating Inequality Constraints

Our final example gives an in-depth overview of using the GHM and Algorithm 6. In this example, we use the University of Michigan’s MARLO [22], [25] (Figure 8(b)) to demonstrate how to incorporate inequality constraints into a continuation. The biped is part of a line of ATRIAS bipeds developed at Oregon State University [55]. The hybrid dynamics of the model is detailed in [25]. We do not model the series-elastic actuators, but do take into account the mass of the actuators. The physical parameters for our model are taken from the source code in [56], which is used in [22].

MARLO has 16 degrees-of-freedom (DOFs) when no constraints are applied. The biped walks in its sagittal plane with gravity pointing downward. Referring to Figure 8(b), the joints of the biped are a 6-DOF floating base (where  $q_1$ – $q_3$  are

the roll, pitch, and yaw angles, respectively), two hip joints for out-of-plane leg rotation ( $q_4$ – $q_5$ ), and eight joints for the two four-bar mechanisms serving as legs for the biped ( $q_6$ – $q_{13}$ ). When constraints are applied, MARLO has seven PHCs ( $n_p = 7$ ). Three of the constraints keep the stance foot (a point) stationary and the other four constraints are the four-bar linkage constraints on each leg:

$$\begin{aligned} q_6 + q_{10} - q_7 &= 0 & q_7 + q_{11} - q_6 &= 0 \\ q_8 + q_{12} - q_9 &= 0 & q_9 + q_{14} - q_8 &= 0. \end{aligned}$$

Given these constraints, we can describe a pre-impact state  $x_0 \in \mathcal{X}$  of the biped using 18 numbers, the nine joint angles  $q_1$ – $q_9$  and their respective velocities ( $n = 9$ ).

The biped has six actuators that drive the robot’s leg joints  $q_4$ – $q_9$  ( $n_u = 6$ ) and is subject to six virtual holonomic constraints ( $n_v = 6$ ). When the left leg is in stance, the constraints are

$$\begin{aligned} q_4 - b_4^3(\theta, a) &= 0 & q_5 - b_5^3(\theta, a) &= 0 & q_6 - b_6^3(\theta, a) &= 0 \\ q_{10} - b_{10}^3(\theta, a) &= 0 & q_8 - b_8^4(\theta, a) &= 0 & q_{12} - b_{12}^4(\theta, a) &= 0, \end{aligned}$$

and similarly when the right leg is in stance.

During a step, the VHCs force the hip, stance thigh, and lower leg to track third-order Bézier polynomials and the swing thigh and lower leg to track fourth-order Bézier polynomials. The two fourth-order polynomials  $b_8^4(\theta, a)$  and  $b_{12}^4(\theta, a)$  each have a free coefficient that is not determined by the periodicity boundary constraints. The two free coefficients, say  $\alpha_1, \alpha_2 \in \mathbb{R}$ , correspond to control dimensions in  $\mathcal{S}$ .

Overall, there are six control parameters  $\mu = [\omega, s_1, s_2, s_3, \alpha_1, \alpha_2]^T \in \mathcal{M} \subseteq \mathbb{R}^k$  ( $k = 6$ ), explained below. The dimensionless parameter  $\omega \in \mathbb{R}$  continuously deforms the physical parameters of the biped from a planar model into a 3D model by controlling the hip width and the position of the center of mass of each link on the biped (in other words, if the hip width is defined by the physical parameter  $\ell_{\text{hip}}$ , then the model would have its hip width defined as the product  $\omega \ell_{\text{hip}}$ ). Figure 9 depicts how  $\omega$  affects the biped’s hip width; it does not show the effects on the center of mass of each link. At  $\omega = 0$ , the biped has zero hip width and all of the center of masses are projected onto their respective links. When  $\omega = 1$ , the original values for the biped’s hip width and link center of masses are restored.

Finally, the vector  $\mu$  has three slack variables  $s_1, s_2, s_3 \in \mathbb{R}$  with lower bounds  $s_1, s_2, s_3 \geq 0$ ; there are no upper bounds on the variables. These constraints are treated as box constraints [42]. We use the slack variables  $s_1$  and  $s_2$  so that we only search for gaits where the knee joints  $q_{10}$  and  $q_{12}$  are nonnegative pre-impact. This is sufficient to avoid knee hyperextension as the biped takes its step ( $q_{10}(t), q_{12}(t) \leq 0$  for all  $t$ ). The third slack variable  $s_3$  is used to make the biped walk from left to right by imposing a forward velocity constraint on the biped’s floating base  $q_y \in \mathbb{R}$  coordinate.

We also impose integral inequality constraints. Let  $p(t) = p(\varphi_\mu^t(x_0)) \in \mathbb{R}^3$  represent the location of the swing foot in space, and  $\text{dist}(p(t)) \in \mathbb{R}$  be a distance function that is positive when the swing foot is above the surface, zero when the swing foot is on the surface, and negative when the swing foot is below the surface. The goal is for the swing foot  $p(t)$  to

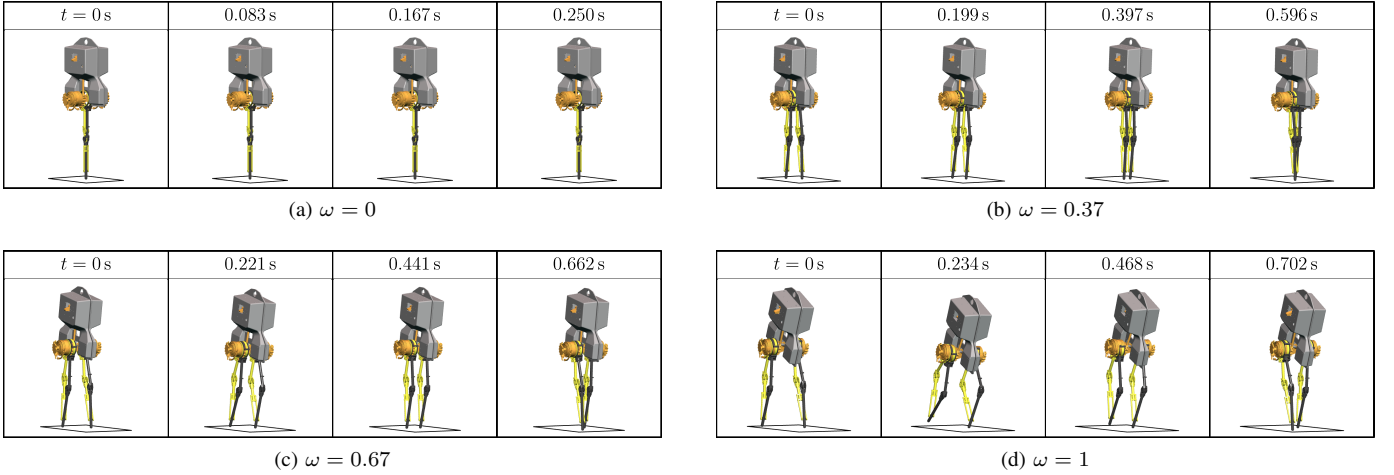


Fig. 9. The effect of the parameter  $\omega$  on the hip width of MARLO. The parameter also affects the position of the center of mass of each link (not shown).

never go below the walking surface. To avoid foot penetration with the ground, we require  $\text{dist}(p(t)) \geq 0$  for all  $t \in \mathbb{R}$ . This is equivalent to finding the zeros of  $\int_0^\tau [\text{dist}(p(t))]^- dt$ , where  $[x]^-$  returns  $x$  if  $x \leq 0$  and zero otherwise.

Given the model and its PHCs and VHCs, the resulting state-time-control space  $\mathcal{S}$  is 25-dimensional (18 state variables, six design and control parameters, and one switching time). The biped's periodicity map  $P$  is

$$P(c) = \begin{bmatrix} Q_1 \\ \dot{Q}_1 \end{bmatrix}, \quad Q_1 = \begin{bmatrix} q_1(\tau^-) - q_1(0^-) \\ q_2(\tau^-) - q_2(0^-) \\ q_3(\tau^-) - q_3(0^-) \end{bmatrix},$$

which states that the roll, pitch, and yaw angles of the floating base have to be periodic. These are the only angles that are unactuated; all other angles are subject to VHCs which we can design to satisfy the periodicity condition of the (virtually) constrained joints [21].

The manifolds in the gait space  $\mathcal{G}$  are 19-dimensional (25 state-time-control variables minus six periodicity constraints). We cannot apply Algorithm 1 because  $\frac{\partial P}{\partial x_0}(c) \in \mathbb{R}^{6 \times 18}$  is not a square matrix. For MARLO, we demonstrate the utility of searching for locomoting gaits on a high-dimensional manifold using a GHM. As an additional benefit of the GHM, we can start from any EG with an arbitrarily chosen switching time  $\tau$  provided the equilibrium gait is not a root of Equation (12).

The primary goal of using the GHM is to generate a gait of the 3D model starting from an EG of the planarized version of biped model ( $\omega = 0$ ). To achieve this goal, we instantiate the map of Equation (13) as  $M_a : \mathcal{S} \rightarrow \mathbb{R}^{18}$  such that

$$M_a(c) = [P^T(c), \Phi^T(c), H^T(c) - p(c)H^T(a)]^T,$$

$$\Phi(c) = \begin{bmatrix} q_6(0^-) - q_7(0^-) - s_1 \\ q_8(0^-) - q_9(0^-) - s_2 \\ \dot{q}_y(0^-) - s_3 \\ q_1(0^-) \\ q_2(0^-) \\ q_4(0^-) \\ q_5(0^-) \end{bmatrix}, \quad H(c) = \begin{bmatrix} s_1 - s_{1,\text{des}} \\ s_2 - s_{2,\text{des}} \\ \sigma(c) - \sigma_{\text{des}} \\ q_y(\tau^-) - q_y(0^-) - q_{y,\text{des}} \\ \int_0^\tau [\text{dist}(p(t))]^- dt \\ \omega - 1 \end{bmatrix},$$

where the map  $P$  is the biped's periodicity map;  $p(c) \in \mathbb{R}$  is the homotopy parameter (Equation (12));  $\Phi : \mathcal{S} \rightarrow \mathbb{R}^7$  is a map of three inequality constraints and four equality constraints,

where the first two constraints ensure the left and right knee joints bend inward in an anthropomorphic manner, the third constraint ensures the biped travels from left to right with a positive forward velocity, and the last four constraints ensure the out-of-plane angles (including those of the floating base) start and end at zero degrees; and, finally, the map  $H : \mathcal{S} \rightarrow \mathbb{R}^6$  is used to find a gait with a desired knee bend ( $s_{1,\text{des}} = s_{2,\text{des}} = 20^\circ$ ), walking surface ( $\sigma_{\text{des}} = 0 \in \mathbb{R}^2$ , i.e., a flat ground), step length ( $q_{y,\text{des}} = 0.5 \text{ m}$ ), minimum height above the ground for the swing foot during a step ( $\text{dist}(p(t)) > 0$ ), and original physical parameters (e.g., a gait in  $\mathcal{G}$  with  $\omega = 1$ ). These are common equality and inequality constraints encountered in the literature [6], [21], [25], [32], [33].

Figure 9 shows the deformation of a gait starting from an EG of  $a = (0, 0.25) \in E$ , where  $a$  corresponds to a planar biped model in its equilibrium stance ( $\omega = 0$ , Figure 9(a)), to a desired gait of the original 3D model ( $\omega = 1$ ) using the map  $M_a$  and Algorithm 6. The Mathematica code found a desired gait after 42 minutes and computed 58 gaits.

## VI. CONCLUSION

We present a robust method for generating large families of walking gaits for high-degree-of-freedom bipeds using numerical continuation methods. Our approach differs from other gait-generation algorithms in that we transform the problem of gait generation to mapping a level set in a state-time-control space. A major advantage is that a one-footed equilibrium stance suffices as a seed to find nearby walking gaits for bipeds subject to physical and virtual holonomic constraints. Furthermore, we prove that the dimension of the search space for an initial gait is one dimensional and is independent of the number of states and controls of the biped. We have applied this approach to find both passive and actuated gaits for a wide variety of simulated bipeds, including the compass-gait, Atlas, and MARLO discussed in this paper.

## ACKNOWLEDGMENT

We thank Jian Shi, Zack Woodruff, and Paul Umbanhowar for their feedback on this paper.

## APPENDIX A BIPEDS AS CONSTRAINED MECHANICAL SYSTEMS

In Section II, we defined the hybrid dynamics  $\Sigma$  as the tuple  $\Sigma = (\mathcal{X}, f, \Delta, \phi)$ , where  $f : \mathcal{X} \times \mathbb{R}^{n_u} \rightarrow T\mathcal{X}$  is a vector field on  $\mathcal{X}$ ,  $\Delta : \mathcal{X} \rightarrow \mathcal{X}$  is a jump map mapping pre- to post-impact states, and  $\phi : \mathbb{R} \times \mathcal{X} \rightarrow \mathbb{R}$  is a switching function which determines when an impact occurs. The goal of this section is to derive  $f$  and  $\Delta$  in terms of the Euler-Lagrange equations for constrained mechanical systems [37], [57], [58].

### A. The Vector Field $f$

We model the continuous dynamics of an  $n$ -degree-of-freedom biped as a constrained mechanical system subject to  $n_p$  PHCs and  $n_v$  VHCs ( $n_p, n_v \geq 0$ ). For a biped's continuous dynamic regime, we assume that the state of the biped  $x = (q, \dot{q}) \in \mathcal{X}$  is known and that the biped is subject to a set of physical and virtual holonomic constraints  $h_p(q) = 0 \in \mathbb{R}^{n_p}$  and  $h_v(q) = 0 \in \mathbb{R}^{n_v}$ , respectively. The state  $x$ , accelerations  $\ddot{q} \in \mathbb{R}^n$ , constraint forces  $\lambda \in \mathbb{R}^{n_p}$ , and control inputs  $u \in \mathbb{R}^{n_u}$  ( $n_u \geq n_v$ ) of the continuous dynamics satisfy

$$\begin{aligned} M(q)\ddot{q} + b(q, \dot{q}) &= J_p^T(q)\lambda + B_v(q)u, \\ J_p(q)\dot{q} + J_p(q)\ddot{q} &= 0, \quad J_v(q)\dot{q} + J_v(q)\ddot{q} = -v(q, \dot{q}), \end{aligned} \quad (14)$$

where  $M(q) \in \mathbb{R}^{n \times n}$  is the mass matrix,  $b(q, \dot{q}) \in \mathbb{R}^n$  is a vector of the centrifugal, Coriolis, and gravitational forces,  $B_v(q) \in \mathbb{R}^{n \times n_u}$  is a transmission matrix,  $J_p(q) = \frac{\partial h_p}{\partial q}(q) \in \mathbb{R}^{n_p \times n}$  and  $J_v(q) = \frac{\partial h_v}{\partial q}(q) \in \mathbb{R}^{n_v \times n}$  are the constraint Jacobian for the physical and virtual constraints, respectively, and  $v(q, \dot{q}) \in \mathbb{R}^{n_v}$  is a linear feedback controller for stabilizing the virtual constraints. An example PD control law for  $v(q, \dot{q})$  used in [21], [32] is

$$v(q, \dot{q}) = \frac{1}{\epsilon} K_D J_v(q)\dot{q} + \frac{1}{\epsilon^2} K_P h_v(q),$$

where  $h_v(q) \in \mathbb{R}^{n_v}$  are VHCs,  $K_P, K_D \in \mathbb{R}^{n_v \times n_v}$  are positive-definite matrices and  $\epsilon \in \mathbb{R}$  is a positive scalar tuning parameter which can speed up convergence to the origin,  $h_v(q) = J_v(q)\dot{q} = 0$ .

Given Equation (14), the vector field  $f$  is then  $f(x, u) = (\dot{q}, \ddot{q})$ , where  $\ddot{q}$  is the solution to

$$\begin{bmatrix} M(q) & -J_p^T(q) & -B(q) \\ J_p(q) & 0 & 0 \\ J_v(q) & 0 & 0 \end{bmatrix} \begin{bmatrix} \ddot{q} \\ \lambda \\ u \end{bmatrix} = - \begin{bmatrix} b(q, \dot{q}) \\ 0 \\ v(q, \dot{q}) + J_v(q)\dot{q} \end{bmatrix},$$

which is a linear system of equations with  $n + n_p + n_v$  equations in  $n + n_p + n_u$  unknowns. A solution exists with a generalized right inverse (we use the Moore-Penrose inverse) as long as the matrix on the left-hand side has maximal rank  $n + n_p + n_v$ .

*Remark 9.* The differential form of the virtual constraints  $J_v(q)\dot{q} + J_v(q)\ddot{q} = -v(q, \dot{q})$  can model virtual holonomic and nonholonomic constraints. The same is true of the differential form of the physical constraints.

*Remark 10.* A linear stabilizing feedback controller  $v_p(q, \dot{q})$  can also be defined for the  $n_p$  physical constraints such that  $J_p(q)\dot{q} + J_p(q)\ddot{q} = -v_p(q, \dot{q})$  in order to reduce constraint

violations during simulations due to numerical rounding errors. For example, we can implement Baumgarte's constraint stabilization technique [59] using the form of the feedback law for  $v(q, \dot{q})$ . Other options also exist [60].

*Remark 11.* The solution to  $u(t)$  of Equation (14) is equivalent to the solution of a stabilizing feedback linearizing control law used to enforce VHCs in the Hybrid Zero Dynamics framework [21] with  $v(q, \dot{q})$  as the linear control law.

### B. The Jump Map $\Delta$

We model collisions as a set of impulsive algebraic equations, namely the impulse-momentum equations in generalized coordinates along with a set of plastic impact equations needed to uniquely solve for the impulse and post-impact velocities. During a collision at time  $t \in \mathbb{R}$ , we assume the pre-impact state of the biped  $x(t^-) = (q, \dot{q}) \in \mathcal{X}$  is known. The pre-impact state  $x(t^-)$ , post-impact state  $x(t^+) = (q^+, \dot{q}^+) \in \mathcal{X}$ , and impulses  $\iota \in \mathbb{R}^{n_u}$  of the impulse equations satisfy

$$q^+ = q, \quad M(q)(\dot{q}^+ - \dot{q}) = J_\iota^T(q)\iota, \quad J_\iota(q)\dot{q}^+ = 0,$$

where  $J_\iota \in \mathbb{R}^{n_u \times n}$  is the constraint Jacobian that maps the post-impact velocities to contact velocities.

The jump map  $\Delta$  is then  $\Delta(x) = (q, \dot{q}^+)$ , where  $\dot{q}^+$  is the solution to

$$\begin{bmatrix} M(q) & -J_\iota^T(q) \\ J_\iota(q) & 0 \end{bmatrix} \begin{bmatrix} \dot{q}^+ \\ \iota \end{bmatrix} = \begin{bmatrix} M(q)\dot{q} \\ 0 \end{bmatrix},$$

which is a linear system of equations with  $n + n_\iota$  equations in  $n + n_\iota$  unknowns. A unique solution exists as long as  $J_\iota$  has maximal rank  $n_\iota$ .

For most bipeds,  $J_\iota = J_p$ . In general, any  $J_\iota$  is fine as long as the set of jump map constraints are more restrictive than the PHC constraints, i.e.,  $\{x \in \mathcal{X} : J_\iota(q)\dot{q}\} \subseteq \{x \in \mathcal{X} : J_p(q)\dot{q}\}$ .

## APPENDIX B

### DEBUGGING ERROR MESSAGES FROM ALGORITHM 4

When a call to Algorithm 4 results in an error state, the following are a list of potential sources of errors and solutions.

#### A. If the plot of $I(\tau)$ is the constant zero line $I(\tau) = 0$

In this case, the output indicates that equilibrium branches in the state-time subspace are not one dimensional. In other words, there exists a configuration parameter, similar to the switching time, that can be varied while still keeping the robot at an equilibrium configuration. For example, Atlas' wrist joints about the  $x$  axis can be continuously rotated creating a three-dimensional branch of equilibrium gaits parameterized by the switching time and the two joint parameters. For this case, we recommend

- 1) checking the model as the free parameter might be due to a joint, as in Atlas' case. A few potential solutions are to remove the corresponding periodicity constraint, specify a trajectory for the joint to follow using a VHC, or keep the joint locked using a VHC, and
- 2) removing redundant periodicity constraints; a periodicity constraint is redundant if there exists another periodicity constraint or VHC that already makes the joint track a periodic trajectory. This can often also lead to the elimination of a state or control parameter.

### B. If the plot has no zero crossings $I(\tau) \neq 0$

This situation can occur for several reasons, including

- 1) the search window is too small, in which case, increase it,
- 2) the biped may have sufficient control authority (see Remark 7). We recommend proceeding in a manner similar to the example with MARLO, which uses Algorithm 6, or
- 3) singular points may not exist on the equilibrium branch being searched; based on experience, we typically assume a search window of  $\tau \in [0, 1]$  (in seconds) is sufficient to assume that there are no singular points on the equilibrium branch.

## APPENDIX C

### PROOFS OF THE EQUILIBRIUM BRANCHES OF $M_0$

*Proof of Proposition 1.* It follows from the implicit function theorem (IFT, [35]) that there exists a unique curve  $c$  passing through  $c_0$ . What remains to be shown is that the points on the curve are all in  $E_0$ . From the IFT, we conclude that in an open neighborhood  $A \subseteq \mathbb{R}$  containing  $\tau_0$  and an open neighborhood  $B \subseteq \mathbb{R}^{2n+k}$  containing the pair  $(x_{\text{eq}}, \mu_0)$  that for each  $\tau(s) \in A$  there exists a unique  $g(\tau(s)) \in B$  such that  $g(\tau) = (x_0(\tau), \mu_0(\tau))$ ,  $c(s) = (x_0(\tau(s)), \tau(s), \mu_0(\tau(s)))$  and  $M_0(c(s)) = 0$  for some parameterization of  $s \in (-\delta, \delta)$ .

We determine  $g$  from the Jacobian  $J_0$  of  $M_0$

$$J_0(c) = \begin{bmatrix} \frac{\partial P}{\partial c}(c) \\ \frac{\partial \Phi_0}{\partial c}(c) \end{bmatrix} = \begin{bmatrix} \frac{\partial P}{\partial x_0}(c) & \frac{\partial P}{\partial \tau}(c) & \frac{\partial P}{\partial \mu}(c) \\ 0 & 0 & I_k \end{bmatrix}. \quad (15)$$

Given that  $x_{\text{eq}}$  is an equilibrium point, we have at  $J(c_0)$

$$\frac{\partial P}{\partial \tau}(p(s_0)) = f(x_{\text{eq}}, u(\tau(s_0))) \frac{\partial \tau}{\partial c}(p(s_0)) = 0.$$

Additionally, because  $c_0$  is a regular point of  $M_0$ , the submatrix

$$\bar{J} = \begin{bmatrix} \frac{\partial P}{\partial x_0}(c_0) & \frac{\partial P}{\partial \mu}(c_0) \\ 0 & I_k \end{bmatrix}$$

must be full rank,  $\det(\bar{J}) \neq 0$ , or else  $J_0$  cannot have maximal rank and  $c_0$  would be a singular point, which it is not. From these two facts, the IFT states that  $g$  must be the solution to the IVP

$$g(\tau_0) = (x_{\text{eq}}, \mu_0),$$

$$\frac{\partial g}{\partial \tau}(\tau) = - \begin{bmatrix} \frac{\partial P}{\partial x_0}(p(s_0)) & \frac{\partial P}{\partial \mu}(p(s_0)) \\ 0 & I_k \end{bmatrix}^{-1} \begin{bmatrix} \frac{\partial P}{\partial \tau}(p(s_0)) \\ 0 \end{bmatrix} = 0,$$

which gives  $g(\tau(s)) = (x_{\text{eq}}, \mu_0)$  for all  $\tau(s) \in \mathbb{R}$ .

To finish describing the curve  $c$ , we now determine an expression for  $\tau = \tau(s)$  valid for  $s \in (-\delta, \delta)$ . Given an arclength parameterization of the curve  $c$ , the tangent to the curve  $c$  at  $c_0$  is  $\frac{dc}{ds}(0)$  and it is the only vector in the tangent space  $T_{c_0} M_0$ . As the tangent space is equal to the null space of  $J_0(c_0)$ , we have

$$\text{Null}(J_0(c_0)) = \text{Null} \left( \begin{bmatrix} \frac{\partial P}{\partial x_0}(c) & 0 & \frac{\partial P}{\partial \mu}(c) \\ 0 & 0 & I_k \end{bmatrix} \right)$$

$$= \{[0_{2n}, \ 1, \ 0_k]^T\},$$

where  $0_k$  and  $0_{2n}$  are vectors with  $k$  and  $2n$  zeros, respectively. Hence,  $\frac{d\tau}{ds}(s) = 1$  and for  $\tau(0) = \tau_0$ ,  $\tau(s) = \tau_0 + s$ .

Therefore,  $c(s) = (x_{\text{eq}}, \tau_0 + s, \mu_0)$  for  $s \in (-\delta, \delta)$ , which are all in  $E_0$  and by the IFT are the only points in a neighborhood containing  $c_0$  that are in  $\mathcal{G}_0$ .  $\square$

*Proof of Proposition 2.* We prove the first claim by showing that the path  $p$  can never have points in  $\mathcal{G}_0 - E_0$  if EGs on the path are regular points of  $M_0$ . The second claim is proven through a direct computation.

Assume there exists a path  $p$  with  $p(0) \in E_0$  and  $p(1) \in \mathcal{G}_0 - E_0$  such that all EGs in  $p$  are regular points of  $M_0$ . Then by Proposition 1 because  $c_0 \in E_0$  is a regular point of  $M_0$ , any path  $p : [0, 1] \rightarrow \mathcal{G}_0$  starting at  $c_0$  must coincide locally with the unique curve  $c : (-\delta, \delta) \rightarrow E_0$ . As the functions  $p$  and  $c$  coincide but have different domains, assume that  $s \in [0, s_\delta)$  continuously maps to  $\alpha(s) \in (-\delta, \delta)$  such that for  $s = 0$  we have  $\alpha(0) = 0$ .

Consider  $p$  at  $s = s_\delta$ . Because  $p$  is continuous  $p(s_\delta)$  must be equal to the left-sided limit of  $p$  at  $s_\delta$ , that is,  $p(s_\delta) = \lim_{s \nearrow s_\delta} (x_{\text{eq}}, \tau_0 + \alpha(s), \mu_0) = (x_{\text{eq}}, \tau_0 + \alpha(s_\delta), \mu_0)$ . Therefore,  $p(s_\delta)$  is an EG in  $E_0$ , but by assumption it is also a regular point of  $M_0$ , so we can apply Proposition 1 and conclude that the interval over which  $p$  and  $c$  have to coincide extends beyond  $s \in (0, s_\delta)$  for the path  $p$ .

In other words, the unique curve  $c$  passing through  $c(0)$  can be extended past the open interval  $(-\delta, \delta)$ . In fact, there is no finite value of  $\delta$  that can contain the entire interval of  $c$  as its limit points  $c(\delta) = p(s_\delta) \in E_0$  are regular points of  $M_0$ . The curve can always be extended and as the curve  $c$  is unique, the path  $p$  has no choice but to follow it. The path  $p$  however is finite with its points determined by  $c$  over its finite interval, but, for  $s \in [0, 1]$ ,  $p(s) \in E_0$ . This contradicts our main assumption that  $p(1) \in \mathcal{G}_0 - E_0$  given that all EGs are regular points of  $M_0$ .

Therefore, there must exist at least one singular EG on the path  $p$ . In order for a point  $p(s) \in E_0$  in the path  $p$  to be singular, we need the submatrix  $\bar{J}$  of the Jacobian  $J_0$  evaluated at  $p(s)$

$$\bar{J}(p(s)) = \begin{bmatrix} \frac{\partial P}{\partial x_0}(p(s)) & \frac{\partial P}{\partial \mu}(p(s)) \\ 0 & I_k \end{bmatrix}$$

to not be invertible so that the IFT (and Proposition 1) does not apply. For any  $p(s)$  that is a singular EG of  $M_0$ , this can only happen if

$$\det \left( \begin{bmatrix} \frac{\partial P}{\partial x_0}(c_s) & \frac{\partial P}{\partial \mu}(c_s) \\ 0 & I_k \end{bmatrix} \right) = \det \left( \frac{\partial P}{\partial x_0}(c_s) \right) = 0.$$

$\square$

*Proof of Proposition 3.* Given that  $c_0$  is an isolated singular point in  $E_0$ , we must have that there are exactly  $\dim(T_{c_0} \mathcal{G}_0) = 2$  curves that intersect transversally at  $c_0$ . Otherwise, we would conclude that  $c_0$  is not isolated or  $\dim(T_{c_0} \mathcal{G}_0) \neq 2$ , which would be a contradiction. Hence, it suffices to study the tangent space  $T_{c_0} \mathcal{G}_0$  to locally determine the gaits on each curve near  $c_0$ .

From Equation (4), a basis for the tangent space  $T_{c_0} \mathcal{G}_0$  is  $T_{c_0} \mathcal{G}_0 = \text{Null}(J_0(c_0))$ , where  $J_0$  is the Jacobian of

$M_0$  (Equation (8)). Because  $c_0$  is a singular EG, we have from Corollary 1 and Proposition 2 that  $\frac{\partial P}{\partial \tau}(c_0) = 0$  and  $\det(\frac{\partial P}{\partial x_0}(c_0)) = 0$ . This implies that the null space of  $J_0(c_0)$  has at least two linearly independent tangent vectors and, by assumption of the above proposition, it has exactly two. As  $\frac{\partial P}{\partial \tau}(c_0) = 0$ , the Jacobian  $J_0$  evaluated at  $c_0$  has the form

$$J_0(c_0) = \begin{bmatrix} \frac{\partial P}{\partial x_0}(c_0) & 0 & \frac{\partial P}{\partial \mu}(c_0) \\ 0 & 0 & I_k \end{bmatrix}.$$

Assuming coordinates  $(x_0, \tau, \mu)$ , a basis for the null space is  $\text{Null}(J_0(c_0)) = \{e_0, g_0\}$ , where  $e_0 = [0_{2n}, 1, 0_k]^T \in \mathbb{R}^{2n+k+1}$ ,  $g_0$  satisfies  $g_0^T e_0 = 0$ , and  $0_a$  is a row vector of  $a$  zeros. The tangent vector  $e_0$  is in  $TE_0$ . A curve  $c_1$  with tangent vector  $\frac{dc_1}{ds}(0) = e_0$  at  $c_1(0) = c_0$  can only have points of the form  $c_1(s) = (x_{\text{eq}}, \tau_0 + s, \mu_0)$  for  $s \in [-\epsilon, \epsilon]$ . The tangent vector  $g_0$  is orthogonal to  $e_0$ , hence a curve  $c_2$  with  $c_2(0) = c_0$  and  $\frac{dc_2}{ds}(0) = g_0$  has gaits  $c_2(s)$  in  $\mathcal{G}_0 - E_0$  for small values of  $s \neq 0$ .  $\square$

## REFERENCES

- [1] R. D. Gregg, Y. Y. Dhaher, A. Degani, and K. M. Lynch, "On the mechanics of functional asymmetry in bipedal walking," *IEEE Transactions on Biomedical Engineering*, vol. 59, no. 5, pp. 1310–1318, May 2012.
- [2] J. W. Grizzle, C. Chevallereau, R. W. Sime, and A. D. Ames, "Models, feedback control, and open problems of 3D bipedal robotic walking," *Automatica*, vol. 50, no. 8, pp. 1955–1988, Aug 2014.
- [3] W. Xi, Y. Yesilevskiy, and C. D. Remy, "Selecting gaits for economical locomotion of legged robots," *The International Journal of Robotics Research*, Nov 2015.
- [4] V. E. H. Chen, "Passive dynamic walking with knees: A point foot model," Master's thesis, Massachusetts Institute of Technology, 2007.
- [5] A. Hereid, E. A. Cousineau, C. M. Hubicki, and A. D. Ames, "3D dynamic walking with underactuated humanoid robots: A direct collocation framework for optimizing hybrid zero dynamics," *2016 IEEE International Conference on Robotics and Automation (ICRA)*, May 2016.
- [6] M. Posa, S. Kuindersma, and R. Tedrake, "Optimization and stabilization of trajectories for constrained dynamical systems," in *Proceedings of the International Conference on Robotics and Automation (ICRA)*, May 2016.
- [7] R. D. Gregg, A. K. Tilton, S. Candido, T. Bretl, and M. W. Spong, "Control and planning of 3-d dynamic walking with asymptotically stable gait primitives," *IEEE Transactions on Robotics*, vol. 28, no. 6, pp. 1415–1423, dec 2012.
- [8] M. S. Motahar, S. Veer, and I. Poulakakis, "Composing limit cycles for motion planning of 3d bipedal walkers," in *2016 IEEE 55th Conference on Decision and Control (CDC)*. IEEE, dec 2016.
- [9] C. Liu, C. G. Atkeson, and J. Su, "Biped walking control using a trajectory library," *Robotica*, vol. 31, no. 2, pp. 311–322, May 2012.
- [10] C. O. Saglam and K. Byl, "Robust policies via meshing for metastable rough terrain walking," in *Proceedings of Robotics: Science and Systems*, Berkeley, USA, July 2014.
- [11] N. Rosa and K. M. Lynch, "Extending equilibria to periodic orbits for walkers using continuation methods," *2014 IEEE/RSJ International Conference on Intelligent Robots and Systems*, Sep 2014.
- [12] —, "Using equilibria and virtual holonomic constraints to generate families of walking gaits," in *Dynamic Walking Conference*, Mariehamn, Finland, Jun. 2017.
- [13] T. McGeer, "Passive dynamic walking," *Int. J. Robotics Research*, vol. 9, no. 2, pp. 62–82, 1990.
- [14] A. Goswami, B. Thuilot, and B. Espiau, "A study of the passive gait of a compass-like biped robot: Symmetry and chaos," *Int. J. Robotics Research*, vol. 17, no. 12, pp. 1282–1301, 1998.
- [15] M. Garcia, A. Chatterjee, A. Ruina, and M. Coleman, "The simplest walking model: Stability, complexity, and scaling," *ASME J. Biomechanical Engineering*, vol. 120, no. 2, pp. 281–288, 1998.
- [16] A. Chatterjee and M. Garcia, "Small slope implies low speed for McGeer's passive walking machines," *Dynamics and Stability of Systems*, vol. 15, no. 2, pp. 139–157, 2000.
- [17] M. Garcia, A. Chatterjee, and A. Ruina, "Efficiency, speed, and scaling of two-dimensional passive-dynamic walking," *Dynamics and Stability of Systems*, vol. 15, no. 2, pp. 75–99, Jun 2000.
- [18] N. Rosa, A. Barber, R. D. Gregg, and K. M. Lynch, "Stable open-loop brachiation on a vertical wall," in *IEEE International Conference on Robotics and Automation*, May 2012, pp. 1193–1199.
- [19] N. Rosa and K. Lynch, "The passive dynamics of walking and brachiating robots: Results on the topology and stability of passive gaits," in *Nature-Inspired Mobile Robotics: Proceedings of the 16th International Conference on Climbing and Walking Robots and the Support Technologies for Mobile Machines*, 2013.
- [20] B. Krauskopf, H. Osinga, and J. Galan-Vioque, *Numerical Continuation Methods for Dynamical Systems: Path Following and Boundary Value Problems*. Springer, 2007.
- [21] E. R. Westervelt, J. W. Grizzle, C. Chevallereau, J. H. Choi, and B. Morris, *Feedback control of dynamic bipedal robot locomotion*. CRC press Boca Raton, 2007.
- [22] B. Griffin and J. Grizzle, "Nonholonomic virtual constraints for dynamic walking," *2015 54th IEEE Conference on Decision and Control (CDC)*, Dec 2015. [Online]. Available: <http://dx.doi.org/10.1109/CDC.2015.7402850>
- [23] K. A. Hamed, B. G. Buss, and J. W. Grizzle, "Exponentially stabilizing continuous-time controllers for periodic orbits of hybrid systems: Application to bipedal locomotion with ground height variations," *The International Journal of Robotics Research*, vol. 35, no. 8, pp. 977–999, Jul 2016.
- [24] C. Chevallereau, G. Abba, Y. Aoustin, F. Plestan, E. R. Westervelt, C. Canudas-de-Wit, and J. W. Grizzle, "Rabbit: A testbed for advanced control theory," *IEEE Control Systems Magazine*, vol. 23, no. 5, pp. 57–79, 2003.
- [25] A. Ramezani, J. W. Hurst, K. Akbari Hamed, and J. W. Grizzle, "Performance analysis and feedback control of ATRIAS, a three-dimensional bipedal robot," *Journal of Dynamic Systems, Measurement, and Control*, vol. 136, no. 2, p. 021012, Dec 2013. [Online]. Available: <http://dx.doi.org/10.1115/1.4025693>
- [26] C. O. Saglam and K. Byl, "Meshing hybrid zero dynamics for rough terrain walking," in *IEEE International Conference on Robotics and Automation*. IEEE, May 2015.
- [27] W. C. Rheinboldt, "Numerical continuation methods: a perspective," *Journal of Computational and Applied Mathematics*, vol. 124, no. 1–2, pp. 229–244, Dec 2000.
- [28] L. Liu, K. Yin, M. van de Panne, and B. Guo, "Terrain runner: Control, parameterization, composition, and planning for highly dynamic motions," *ACM Trans. Graph.*, vol. 31, no. 6, pp. 154:1–154:10, Nov. 2012.
- [29] Z. Gan, Y. Yesilevskiy, P. Zaytsev, and C. D. Remy, "All common bipedal gaits emerge from a single passive model," *Journal of The Royal Society Interface*, vol. 15, no. 146, Sep. 2018.
- [30] P. E. Gill, W. Murray, and M. A. Saunders, "SNOPT: An SQP algorithm for large-scale constrained optimization," *SIAM Journal on Optimization*, vol. 12, no. 4, pp. 979–1006, Jan 2002. [Online]. Available: <http://dx.doi.org/10.1137/S1052623499350013>
- [31] J. T. Betts, *Practical Methods for Optimal Control and Estimation Using Nonlinear Programming*, 2nd ed. Society for Industrial & Applied Mathematics (SIAM), Jan 2010. [Online]. Available: <http://dx.doi.org/10.1137/1.9780898718577>
- [32] A. Hereid, C. M. Hubicki, E. A. Cousineau, and A. D. Ames, "Dynamic humanoid locomotion: A scalable formulation for HZD gait optimization," *IEEE Transactions on Robotics*, vol. 34, no. 2, pp. 370–387, apr 2018.
- [33] G. Bessonnet, P. Seguin, and P. Sardain, "A parametric optimization approach to walking pattern synthesis," *The International Journal of Robotics Research*, vol. 24, no. 7, pp. 523–536, Jul 2005. [Online]. Available: <http://dx.doi.org/10.1177/0278364905055377>
- [34] N. Rosa, "Bipedal gait generation library," <https://github.com/nr-codes/BipedalGaitGeneration>, 2020, last accessed 6/03/20.
- [35] M. Spivak, *Calculus on Manifolds. A modern approach to classical theorems of advanced calculus*. W. A. Benjamin, Inc., New York-Amsterdam, 1965.
- [36] E. Allgower and K. Georg, *Numerical Continuation Methods, An Introduction*. New York, NY: Springer-Verlag New York, Inc., 1990.
- [37] H. Choset, K. M. Lynch, S. Hutchinson, G. A. Kantor, W. Burgard, L. E. Kavraki, and S. Thrun, *Principles of Robot Motion: Theory, Algorithms, and Implementations*. Cambridge, MA: MIT Press, June 2005.
- [38] S. H. Collins and A. L. Ruina, "A bipedal walking robot with efficient and human-like gait," in *IEEE Int. Conf. on Robotics and Automation*, Barcelona, Spain, 2005, pp. 1983–1988.

- [39] D. Bainov and P. Simeonov, *Impulsive Differential Equations: Periodic Solutions and Applications (Monographs and Surveys in Pure and Applied Mathematics)*. Chapman and Hall/CRC, 1993.
- [40] W. H. Press, S. A. Teukolsky, W. T. Vetterling, and B. P. Flannery, *Numerical Recipes in C: The Art of Scientific Computing*, 2nd ed. Cambridge University Press, 2002. [Online]. Available: <http://apps.nrbook.com/c/index.html>
- [41] M. E. Henderson, "Multiple parameter continuation: Computing implicitly defined k-manifolds," *International Journal of Bifurcation and Chaos*, vol. 12, no. 03, pp. 451–476, Mar. 2002.
- [42] J. Nocedal and S. J. Wright, *Numerical Optimization*. Springer Verlag, 1999.
- [43] D. P. Bertsekas, "Projected Newton methods for optimization problems with simple constraints," *SIAM Journal on Control and Optimization*, vol. 20, no. 2, pp. 221–246, Mar. 1982.
- [44] C. Kelley, *Iterative Methods For Optimization*. Society for Industrial and Applied Mathematics, 1999.
- [45] H. B. Keller, "Global homotopies and Newton methods," *Recent Advances in Numerical Analysis*, pp. 73–94, 1978. [Online]. Available: <http://dx.doi.org/10.1016/B978-0-12-208360-0.50009-7>
- [46] A. Ben-Israel, "A Newton-Raphson method for the solution of systems of equations," *Journal of Mathematical Analysis and Applications*, vol. 15, no. 2, pp. 243–252, aug 1966.
- [47] A. E. Martin, D. C. Post, and J. P. Schmiedeler, "Design and experimental implementation of a hybrid zero dynamics-based controller for planar bipeds with curved feet," *International Journal of Robotics Research*, vol. 33, no. 7, pp. 988–1005, 2014.
- [48] P. X. M. La Hera, A. S. Shiriaev, L. B. Freidovich, U. Mettin, and S. V. Gusev, "Stable walking gaits for a three-link planar biped robot with one actuator," *IEEE Transactions on Robotics*, vol. 29, no. 3, pp. 589–601, Jun 2013.
- [49] R. Dumas, L. Cheze, and J.-P. Verriest, "Adjustments to McConville et al. and Young et al. body segment inertial parameters," *Journal of Biomechanics*, vol. 40, no. 3, pp. 543–553, 2007.
- [50] C. Chevallereau, J. W. Grizzle, and C. Shih, "Asymptotically stable walking of a five-link underactuated 3D bipedal robot," *IEEE Trans. Robotics*, vol. 25, no. 1, pp. 37–50, 2008.
- [51] Boston Dynamics, "Atlas - The Agile Anthropomorphic Robot," [http://www.bostondynamics.com/robot\\_Atlas.html](http://www.bostondynamics.com/robot_Atlas.html), 2013, last accessed 12/4/14.
- [52] R. Featherstone, *Rigid Body Dynamics Algorithms*. Springer, 2007.
- [53] F. Iida and R. Tedrake, "Minimalistic control of a compass gait robot in rough terrain," in *IEEE International Conference on Robotics and Automation*, May 2009, pp. 1985–1990.
- [54] Open Source Robotics Foundation, "drc\_skeleton\_v3\_mod1.cfg," DARPA Robotics Challenge Simulator, default branch commit dfb3482, June 2014.
- [55] C. Hubicki, J. Grimes, M. Jones, D. Renjewski, A. Spröwitz, A. Abate, and J. Hurst, "Atrias: Design and validation of a tether-free 3d-capable spring-mass bipedal robot," *The International Journal of Robotics Research*, vol. 35, no. 12, pp. 1497–1521, 2016.
- [56] B. Griffin, "Nhvc3dsim\_bag160728.zip," [http://www.griffb.com/s/NHVC3DSim\\_BAG160728.zip](http://www.griffb.com/s/NHVC3DSim_BAG160728.zip), 2016.
- [57] G. Liu and Z. Li, "A unified geometric approach to modeling and control of constrained mechanical systems," *IEEE Transactions on Robotics and Automation*, vol. 18, no. 4, pp. 574–587, Aug. 2002.
- [58] F. Aghili, "A unified approach for inverse and direct dynamics of constrained multibody systems based on linear projection operator: Applications to control and simulation," *IEEE Trans. on Robotics*, vol. 21, no. 5, pp. 834–849, 2005.
- [59] O. A. Bauchau and A. Laulusa, "Review of contemporary approaches for constraint enforcement in multibody systems," *Journal of Computational and Nonlinear Dynamics*, vol. 3, no. 1, 2008. [Online]. Available: <http://dx.doi.org/10.1115/1.2803258>
- [60] J. C. Chiou and S. D. Wu, "Constraint violation stabilization using input-output feedback linearization in multibody dynamic analysis," *Journal of Guidance, Control, and Dynamics*, vol. 21, no. 2, pp. 222–228, Mar 1998.